

OPTICAL DETERMINATION OF METAL-SEMICONDUCTOR SCHOTTKY BARRIERS

by



STEPHEN KWOK-WAH CHENG

A Thesis Submitted in Partial Fulfillment of the Requirements  
for the DEGREE OF MASTER OF SCIENCE

DEPARTMENT OF PHYSICS  
LAKEHEAD UNIVERSITY  
THUNDER BAY, ONTARIO, CANADA

AUGUST 1982

ProQuest Number: 10611666

All rights reserved

INFORMATION TO ALL USERS

The quality of this reproduction is dependent upon the quality of the copy submitted.

In the unlikely event that the author did not send a complete manuscript and there are missing pages, these will be noted. Also, if material had to be removed, a note will indicate the deletion.



ProQuest 10611666

Published by ProQuest LLC (2017). Copyright of the Dissertation is held by the Author.

All rights reserved.

This work is protected against unauthorized copying under Title 17, United States Code  
Microform Edition © ProQuest LLC.

ProQuest LLC.  
789 East Eisenhower Parkway  
P.O. Box 1346  
Ann Arbor, MI 48106 - 1346

THESES  
M.Sc.  
1982  
C52



(c) Stephen Kwok-Wah Cheng 1982

## ACKNOWLEDGEMENTS

It gives me great pleasure to thank my research supervisor, Dr. W.J. Keeler, for his assistance and instruction throughout this project.

Special thanks are due to Dr. M. Hawton for her interest in the computer programme concerning the data analysis.

This project is a continuation of work begun by Mr. Anwar-ul-Haque, and his help in sample preparation is greatly appreciated.

I wish to express my appreciation to Mr. G.C. Anderson for his technical help and assistance.

Finally, I wish to thank Mrs. J. Boucher for typing this thesis.

## TABLE OF CONTENTS

	page
LIST OF FIGURES.....	i
LIST OF TABLES.....	iii
ABSTRACT.....	1
INTRODUCTION.....	2
CHAPTER I        THEORETICAL CONSIDERATIONS.....	4
1.1        Models of Barrier Formation.....	4
1.2        Measurement of Schottky Barrier Heights...	8
a) I-V measurements.....	8
b) Capacitance-voltage measurements.....	10
c) Photoemission measurements.....	10
1.3        Theory of Photovoltage Production.....	11
1.4        Diode Equation Development.....	12
CHAPTER II       EXPERIMENTAL.....	18
2.1        Sample Preparation.....	18
2.2        Experimental Apparatus.....	19
2.3        Equivalent Circuit Analysis.....	22
2.4        Experimental Procedure.....	25
CHAPTER III      RESULTS AND DISCUSSION.....	28
3.1        General.....	28
3.2        Experimental Results.....	32
3.3        Low Temperature Effects.....	44
CHAPTER IV       CONCLUSION.....	49
REFERENCES.....	52
APPENDIX.....	55

LIST OF FIGURES

FIGURE		page
1	Energy level diagrams of metal-semiconductor contacts.....	7
2	Measurements of Schottky barrier heights.....	9
3	Change in height of the space-charge barrier with polarity of the applied potential at a metal-semiconductor junction for an n-type crystal.....	14
4	A schematic diagram of the experimental layout..	20
5	Equivalent circuit of metal-semiconductor photovoltaic cell.....	23
6	Photovoltages obtained with and without RC effect in both the d.c. and a.c. measurements...	26
7	Photovoltages generated using equation (2.3.2) for a range of $\phi_b$ values with the constant $C'$ (=1) held fixed.....	29
8	The general dependence of the curves on variation in $C'$ for a fixed value of $\phi_b$ as predicted by equation (2.3.2).....	31
9	A plot of log photovoltage vs. temperature for n-InSb:Ag.....	33

FIGURE		page
10	A plot of log photovoltage vs. temperature for p-InSb:Ag(1).....	34
11	A plot of log photovoltage vs. temperature for p-InSb:Ag(2).....	35
12	A plot of log photovoltage vs. temperature for n-InSb:Au.....	38
13	A plot of log photovoltage vs. temperature for p-InSb:Au.....	40
14	A plot of log photovoltage vs. temperature for n-GaAs:Au.....	41
15	A plot of log photovoltage vs. temperature for n-GaAs:Ag.....	43
16	A plot of log photovoltage vs. temperature for n-GaSb:Ag.....	45

LIST OF TABLES

TABLE		page
1	Work functions and electron affinities.....	30
2	Results.....	50

ABSTRACT

The photovoltage produced by a Schottky barrier photocell shows a strong temperature dependence if the barrier is not too large. We have used this temperature dependence to obtain the barrier height for several III-V semiconductor-Au, Ag combinations. The results suggest that a simple Fermi level difference model is most appropriate for many of these small barrier III-V photocells. This appears to be the case, even if the Fermi level difference leads to a barrier greater than the energy gap of the semiconductor.

## INTRODUCTION

Many investigations of the Schottky barrier size have been carried out in recent years. This information is of importance because of the many applications which use the barrier, most notably those involving photovoltage production. Unfortunately, the results from different measuring techniques do not always agree as well as one might like. While most of the barrier heights have been obtained using C-V and I-V measurements, these do not provide very good results when the barrier is small. On the other hand, Fortin et al. [1] and later Roth et al. [2,3] showed that the Schottky barrier height could be determined quite well when the barrier was small if the temperature dependence of the photovoltage was known. This thesis reports on additional measurements where the temperature dependence of the photovoltage is used to obtain the Schottky barrier produced at the interface between gold or silver and several of the III-V semiconductor groups. While many of these barriers have been determined before, some of the results are new. It will be seen that the method is very useful for the case of small barriers in particular.

The thesis begins with a brief review of the models for barrier formation and then develops an expression for

the temperature dependent photovoltage produced by a Schottky barrier exposed to white light. The experimental method is then discussed, followed by the results for several types of photocells. The concluding sections describe some of the advantages and pitfalls of the present method and the results are finally tabulated.

## CHAPTER I - THEORETICAL CONSIDERATIONS

### 1.1 MODELS OF BARRIER FORMATION

When materials with different Fermi levels are brought into contact along an interface layer, charges are transferred from the material with the higher Fermi energy level to that with the lower. This results in the alignment of the Fermi levels at the same energy. The charge layers produced at the interface during Fermi level realignment create an electric field in the interface volume which results in a depletion region. The internal electric field in the depletion region separates mobile charges of opposite sign if they happen to be created there. The argument applies equally well to p-n junctions and Schottky barrier junctions.

Thus a Schottky barrier junction is formed when a metal is brought into contact with a semiconductor. In the samples investigated here, the metal is evaporated onto the semiconductor. This barrier inhibits the free movement of charge across the interface.

Various assumptions are used in trying to explain the measured barriers produced at p-n and Schottky barriers. Some of these will now be discussed.

1. Schottky Barrier as  $\phi_m - \chi_s$ :-

If a metal of work function  $\phi_m$  is brought into contact with a semiconductor of electron affinity  $\chi_s$  and energy gap  $E_g$ , according to Heinsch [4], the barrier formed is

$$\phi_{bn} = \phi_m - \chi_s$$

between the metal and an n-type semiconductor. For the p-type case, the barrier he predicts is

$$\phi_{bp} = (\chi_s - \phi_m + E_g).$$

Thus, he predicts a barrier which would be the difference between the Fermi level positions if the semiconductor is extrinsic.

2. Surface States Dominated Barrier Production:-

If the Fermi level at the interface is pinned by surface state effects, the barrier for an n-type semiconductor may be given as [2,5]

$$\phi_n = (E_g - \phi_0)$$

where  $\phi_0$  is the Fermi level at the interface measured from

the top of the bent valence band. This always predicts a barrier which is less than  $E_g$ .

However, proof that these surface states exist and are responsible for the barrier size is difficult to obtain.

### 3. Absolute Fermi Level Difference:-

Perhaps the simplest and most straightforward assumption one can make is that the barrier should be determined by a difference in the positions of the Fermi levels for the bulk materials [6]. This is very close to the prediction of method 1 but would differ when the semiconductor is intrinsic and its Fermi level is close to the centre of the energy gap.

The types of barriers which must be considered fall into a further classification of two types. Those with the metal work function lying in the semiconductor energy gap and those with it in the semiconductor's conduction or valence band. Many authors have assumed that an ohmic contact would result for the latter case. Assumption 2 above is usually invoked for dealing with this situation.

Fig. 1 illustrates the barriers formed between a metal and an n or p-type semiconductor when  $\phi_m$  lies inside the energy gap of the semiconductor.

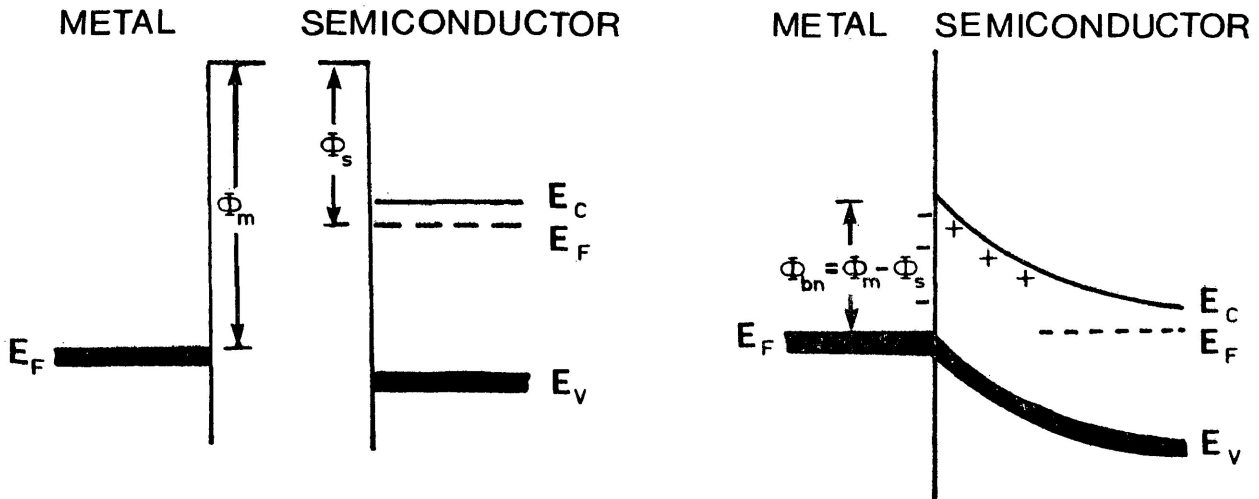


Fig. 1a) Metal contact to an n-type semiconductor with  $\phi_m > \phi_s$ .

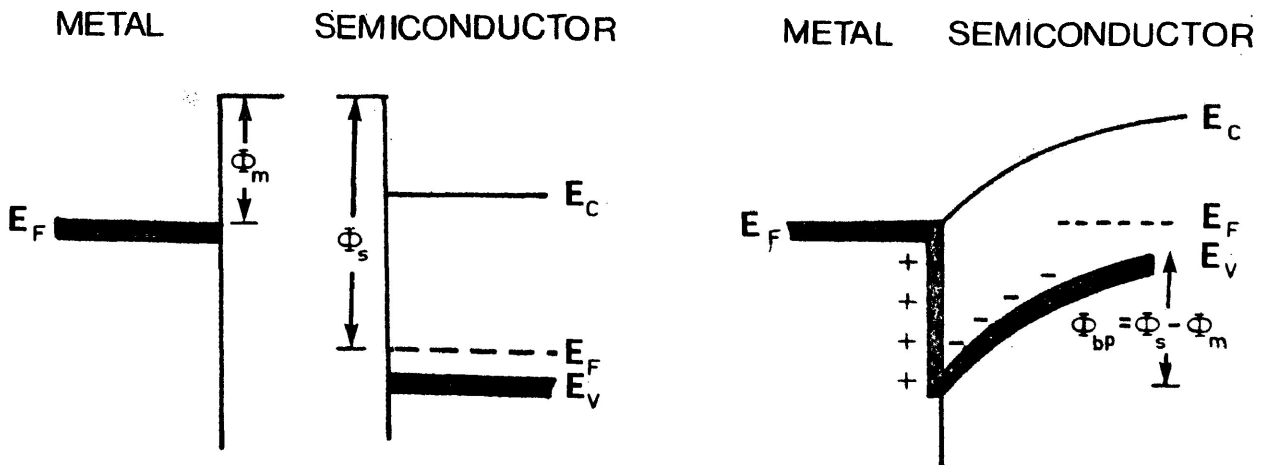


Fig. 1b) Metal contact to a p-type semiconductor with  $\phi_m < \phi_s$ .

FIG. 1. ENERGY LEVEL DIAGRAMS OF METAL-SEMICONDUCTOR CONTACTS

Barrier heights predicted by various models and the uncertainties in the measured values of metal work functions and semiconductor electron affinities, are often of the same magnitude. This makes it difficult to impossible to select the appropriate model in many cases. Thus any method which can add new insight into the process of barrier formation is important.

## 1.2 MEASUREMENT OF SCHOTTKY BARRIER HEIGHTS

There are several methods for measuring the Schottky barrier height [7.8]. Some of the more important methods will now be discussed.

### (a) I-V measurements

Using conventional diode theory (discussed further in section 2.3), one obtains [9] for the current density crossing a barrier  $\phi_b$  in the presence of a biasing voltage V

$$J = J_0 e^{-\phi_b/KT} \left[ e^{qV/KT} - 1 \right] \quad (1.2.1)$$

where  $J_0$  is equal to  $120T^2$  Amp/cm<sup>2</sup> [10], K is Boltzmann's constant,  $\phi_b$  is the barrier, and T is the temperature in Kelvin degrees. The author claims that at room temperature the current density is 1 amp/cm<sup>2</sup> for  $\phi_b - qV$  approximately equal to 0.3 eV. Thus it is possible to estimate  $\phi_b$

FIG. 2. MEASUREMENTS OF SCHOTTKY BARRIER HEIGHTS

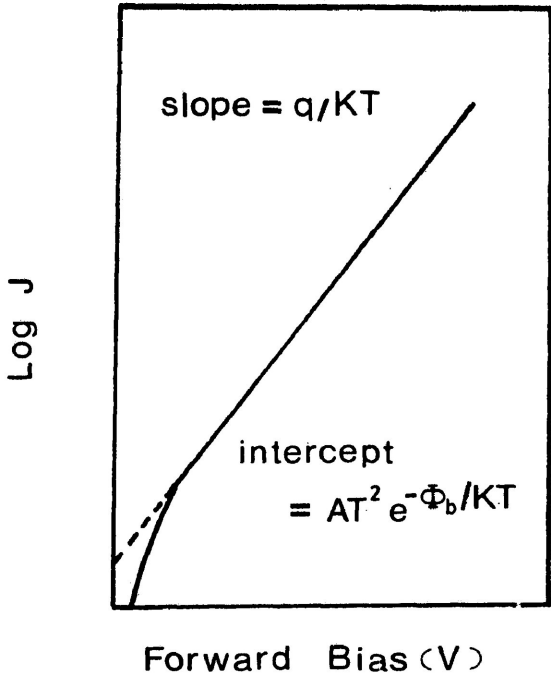


Fig. 2a) Characteristic of forward biased metal semiconductor contact.

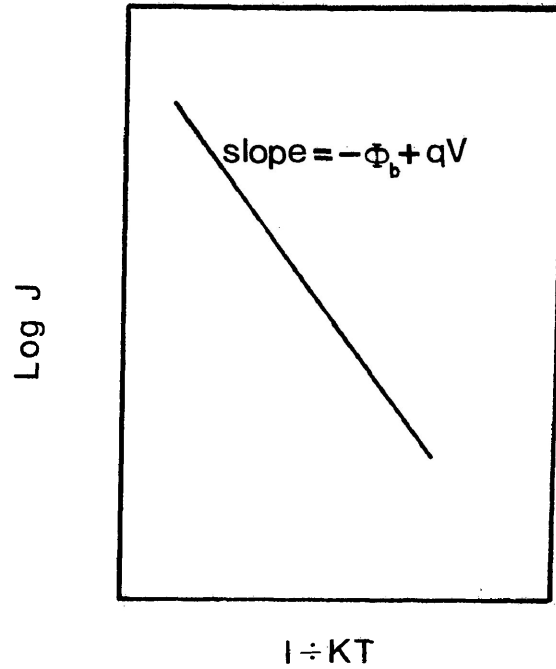


Fig. 2b) Activation energy plot of forward biased metal semiconductor contact.

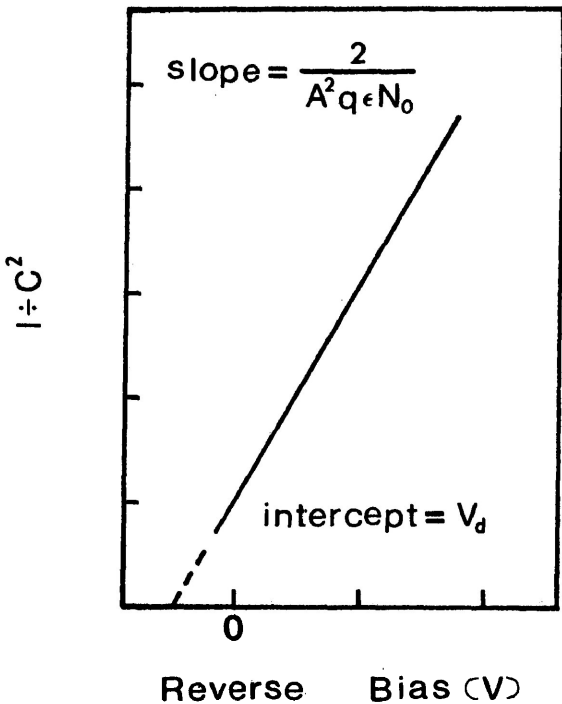


Fig. 2c) Capacitance-voltage characteristic of reverse biased metal semiconductor contact.

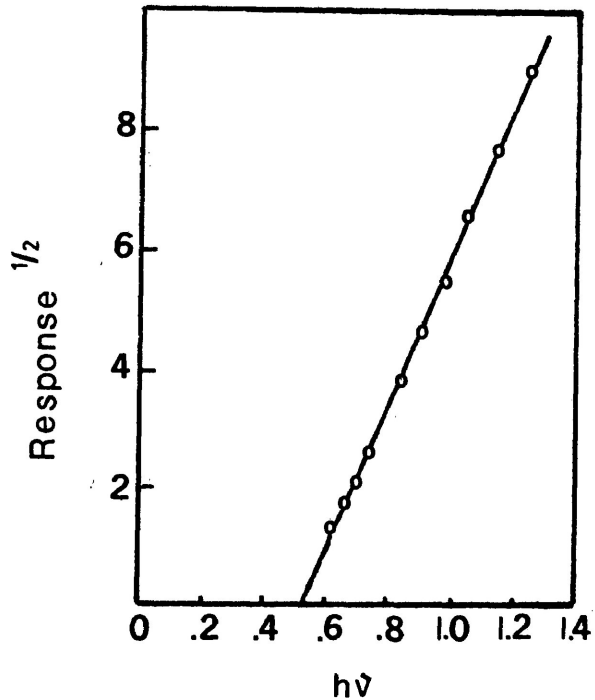


Fig. 2d) Square root of long wavelength photoemission data showing extrapolation to obtain barrier energy.

directly from the I-V curve as shown in Fig. 2a.

Alternately, the thermal activation energy  $\phi_b - qV$  can be determined from the slope of  $\log J$  vs.  $1/T$  as in Fig. 2b.

(b) Capacitance-voltage measurements

When a d.c. bias is placed across the junction the depletion layer is widened. Charge of one sign is placed on the metal surface at the junction interface while charge of the opposite sign is induced on the semiconductor. The capacitance of the junction may be represented by the equation [9]

$$C = \frac{AqN_0 \epsilon^{0.5}}{2(V_d - V)} \quad (1.2.2)$$

To measure this capacitance, a small a.c. voltage can be impressed on the d.c. bias. If  $1/C^2$  is plotted vs. the reverse bias  $-V$  to get the diffusion potential  $V_d$  at the intercept, the barrier height can be determined indirectly from the slope as in Fig. 2c.

(c) Photoemission measurements

Photoemission of electrons in the metal over the barrier provides another method of determining the barrier height. The dependence of the photocurrent  $I$  on the

barrier is predicted to be  $(h\nu - \phi_b)^2$  [9]. If the square root of the photocurrent response is plotted vs. the photon energy, a straight line should result whose intercept is the barrier height  $\phi_b$ .

### 1.3 THEORY OF PHOTOVOLTAGE PRODUCTION

When the Schottky barrier is illuminated by white light some of the incoming photons with energy greater than the semiconductor gap energy will be absorbed in the depletion region where they will create electron-hole pairs. The carriers will move in opposite directions under the influence of the "built-in" electric field and the resulting charge separation produces a potential difference across the junction. This potential difference (V) biases the junction in the forward direction if one uses conventional diode equation concepts.

Recall that the diode equation [9,11]

$$I = I_0 (e^{qV/KT} - 1) \quad (1.3.1)$$

yields the current I under the action of an electrical bias voltage V.  $I_0$  is the thermal reverse saturation current, K is Boltzmann's constant and T is the absolute temperature. In the photovoltaic case, light generates additional carriers

in the junction. Because of the band curvature in the junction region as depicted in Fig. 1 mobile carriers move preferentially in one direction (oppositely for opposite carrier types). This results in the forward biasing of the junction. In addition, some of the carriers recombine before they can be swept away by the built-in field. Under short-circuit load conditions, the current reaching the load will be proportional to this net generation rate of carriers  $G$ . The short-circuit current [12] can thus be given as

$$I_s = Aq(L_e + L_h)G \quad (1.3.2)$$

where  $A$  is the area of the junction,  $L_e$  and  $L_h$  are the electron and hole diffusion lengths and  $G$  is the net carrier generation rate.

#### 1.4 DIODE EQUATION DEVELOPMENT

When the metal and semiconductor are placed in electrical contact their fermi levels must align when equilibrium is established.

If an external potential is applied between the metal and an n-type semiconductor with positive connection

to the semiconductor, the barrier is increased to  $\phi_b + qV$  where  $V$  is the applied potential as in Fig. 3. Since the barrier height is increased by  $qV$  (with respect to vacuum), fewer electrons can flow from the semiconductor to the metal. The barrier height of the metal is unchanged so the current from the metal to the semiconductor is the same. There is a net current flow from the metal to the semiconductor.

When the polarity of the external voltage is reversed, the barrier height is reduced and the current from the semiconductor is increased. Thus there is a net current flow from the semiconductor to the metal. Since the current from the metal is unaffected by the external potential, variation in the current depends on the contribution flowing from the semiconductor. When the current is reduced, the contact is said to be reverse biased and when it is increased it is forward biased.

The current flowing from the metal is determined by the thermionic emission of electrons across the barrier. The current density is [13,14]

$$j(m \text{ to } s) = A_0 T^2 e^{-\phi_b/KT} \quad (1.4.1)$$

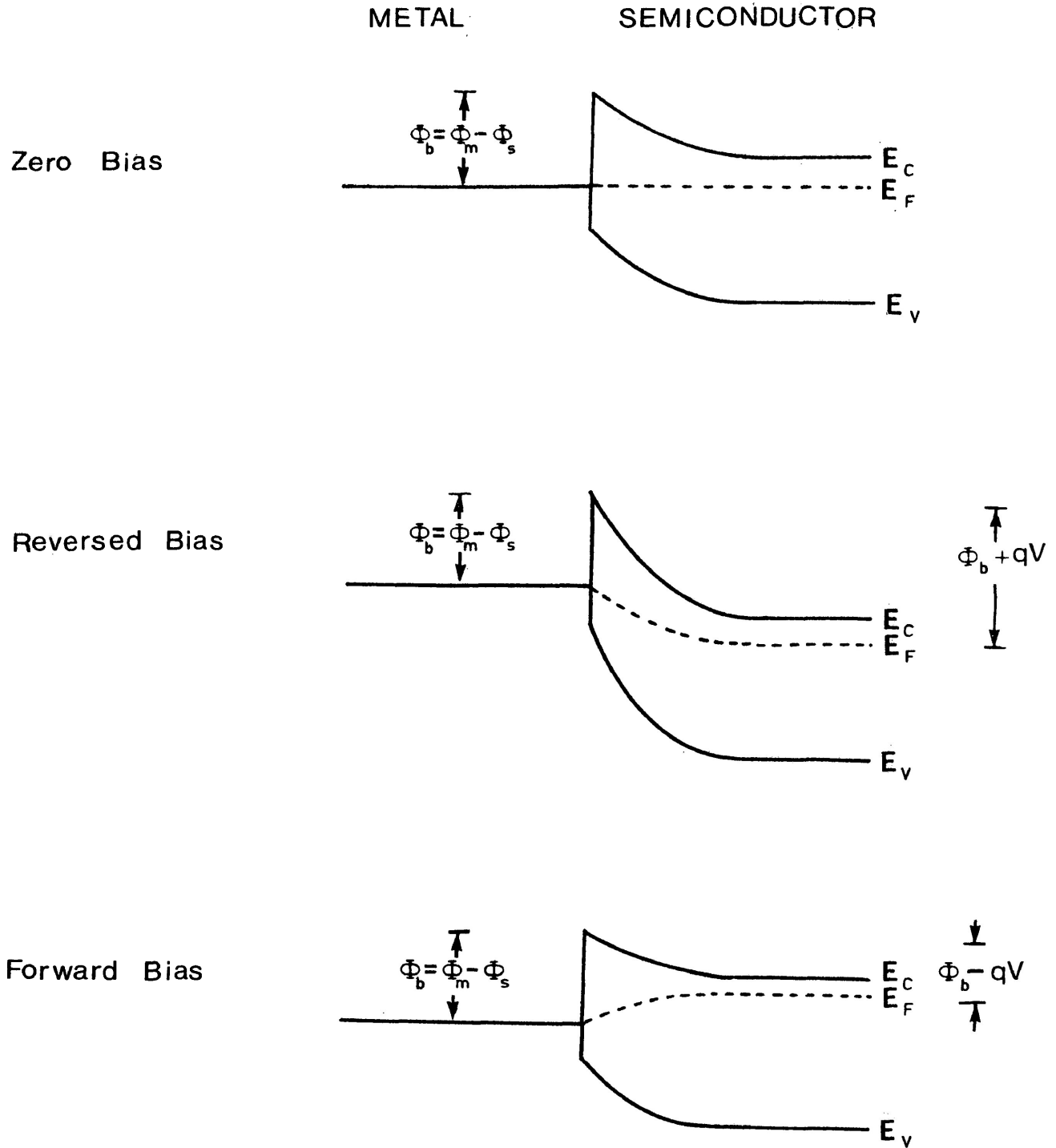


FIG. 3. Change in height of the space-charge barrier with polarity of the applied potential at a metal-semiconductor junction for an n-type crystal.

Similarly, the current flowing from the semiconductor is

$$j(s \text{ to } m) = A_0 T^2 e^{(-\phi_b + qV)/KT} \quad (1.4.2)$$

where  $V$  is the applied potential and  $A_0$  is the Richardson-Dushman constant.

The dark current  $J_\ell$  is given by [9,11]

$$\begin{aligned} J_\ell &= j(s \text{ to } m) - j(m \text{ to } s) \\ &= A_0 T^2 e^{-(\phi_b - qV)/KT} - A_0 T^2 e^{-\phi_b/KT} \\ &= J_0 (e^{qV/KT} - 1) \end{aligned} \quad (1.4.3)$$

where  $J_0 = A_0 T^2 e^{-\phi_b/KT}$

The photovoltaic current density  $J$  is then

$$\begin{aligned} J &= J_s - J_\ell \\ &= J_s - J_0 (e^{qV/KT} - 1) \end{aligned} \quad (1.4.4)$$

where  $J_s$  is the short circuit current density.

When light shines on a junction, electron-hole pairs are created if photons with enough energy are absorbed. Separation of these carriers by the field region results in a forward biasing of the junction. Under no load conditions ( $J = 0$ ) this voltage should be given by the same expression as would be used for an electrically forward biased junction. That is,

$$\begin{aligned} V_{oc} &= (KT/q) \ln \left[ 1 + J_s/J_o \right] \\ &= (KT/q) \ln \left[ 1 + (C^*/T^2) e^{\phi_b/KT} \right] \end{aligned} \quad (1.4.5)$$

where  $C^* = J_s/A_o$ .

At low temperatures  $(C^*/T^2) e^{\phi_b/KT}$  is much greater than 1, the open circuit voltage can then be approximated as

$$V_{oc} = (KT/q) \ln(C^*/T^2) + \phi_b/q \quad (1.4.6)$$

Applying L'Hospital's Rule to the first term as  $T$  goes to zero, we find

$$\begin{aligned} \lim_{T \rightarrow 0} (K/q) \ln(C^*/T^2) / (T^{-1}) \\ = 2KT/q. \end{aligned}$$

Thus, as  $T$  tends to zero, one expects from the above to find

$$V_{oc} = 2KT/q + \phi_b/q = \phi_b/q.$$

## CHAPTER II - EXPERIMENTAL

### 2.1 SAMPLE PREPARATION

Samples were cut from single crystal material using a continuous loop wire saw and a silicon carbide in oil slurry. The samples were approximately  $1 \times 3 \times 5 \text{ mm}^3$ . Cleaning at the various stages was accomplished using trichloroethylene and/or ethanol. The front surfaces were polished using 600 grit compound and oil. After cleaning the samples were etch polished in a fume hood, using a 5% solution of bromine in methanol. The resulting surface was very smooth and shiny.

A metal with a high diffusion coefficient was selected [15,16] for evaporation onto the back surface of each sample to make an ohmic contact. Indium was used for contacting indium antimonide and gallium antimonide, while tin and gold both proved successful in contacting gallium arsenide. During all evaporations, a movable baffle blocked early stage evaporation to prevent volatile impurities from contaminating the sample.

To produce the ohmic semiconductor contact, the samples were either heated in a Micro-Bar miniature furnace through which Argon gas was slowly streamed, or in a Lind-

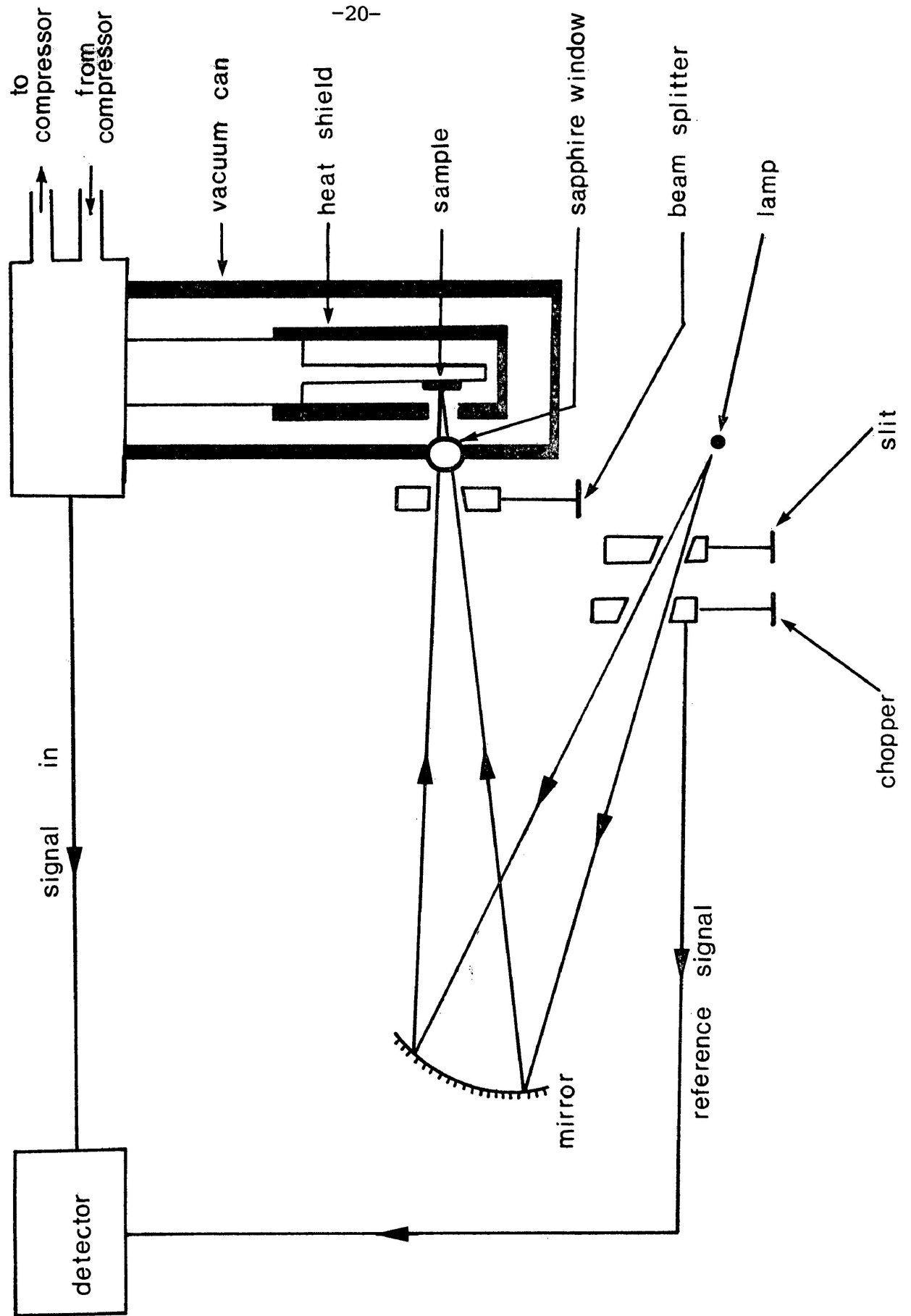
berg heavy-duty furnace under vacuum inside a pumped quartz tube. The Micro-Bar furnace could reach temperatures of approximately  $400^{\circ}\text{C}$  while the Lindberg furnace was capable of much higher temperatures. The InSb samples were heated to about  $200^{\circ}\text{C}$  in the Micro-Bar furnace for five minutes. The diffusion process could be observed visually as temperature was raised. Diffusion into the GaAs and GaSb had to be carried out at  $750^{\circ}\text{C}$  and  $600^{\circ}\text{C}$  respectively, so the Lindberg furnace was employed. Diffusion heating lasted approximately 20 minutes for these samples.

After the diffusion process, each sample was again etch polished. Gold or silver was evaporated onto the front surface as a semi-transparent layer in a vacuum of roughly  $10^{-6}$  torr for barrier formation. Gold appeared to be bluish-green at the thickness used. Platinum wire of 1 mil thickness and silver paste were used to contact the sample on both front and back. The sample was then mounted onto the sample holder of the cryostat and thermally bonded using high thermal conductivity grease.

## 2.2 EXPERIMENTAL APPARATUS

Fig. 4 presents a schematic drawing of the experimental equipment. The cryogenic refrigerator was an Air

FIG. 4. A schematic diagram of the experimental layout.



Products model Displex 208W two-staged, closed-cycle helium refrigerator. It is capable of 30 watts cooling power at 80°K, 10 watts cooling power at 20°K and a low temperature limit of approximately 7°K. When in the use the refrigerator provides two separate stages of adiabatic expansion with the second expansion occurring at the lowest temperature in the system for any particular operating point. Enclosing these expansion stages in high vacuum allowed the system to cool. The temperature of the sample was measured using an NBS calibrated GaAs diode thermometer. Temperature was accurate to within 0.5°K.

White light was chopped and focused through sapphire windows onto the sample. A calibrated proportional beam splitter could be inserted into this beam to reduce the light intensity if needed. Output photovoltage from the sample could be monitored on an oscilloscope. The oscilloscope was used for general setup and beam alignment. It provided a useful means of observing the signal wave shape and hence could be used to detect the presence of unacceptable time constants due to poor sample contacting or lead detachment. The actual recorded signal levels were determined, however, using an Ithaco 393 lock-in detector.

### 2.3 EQUIVALENT CIRCUIT ANALYSIS

The Norton equivalent circuit of a metal semiconductor photovoltaic cell is illustrated in Fig. 5. Following the usual procedure [17-19] the maximum photocurrent is represented by  $I_s$  and the barrier introduces a nonlinear impedance  $Z$ . The shunt resistance  $R_b$  can be caused by ohmic shorts through the barrier or by conduction through the interface along dislocations or grain boundaries. Series resistance  $R_s$  arises in the metal film resistance and in the semiconductor bulk resistance. To prevent loading of the sample photovoltage, the detector input resistance must always be several orders of magnitude greater than the source impedance of the sample. This turned out to be a significant problem when dealing with wide gap semiconductors, particularly at low temperature. As described earlier, the temperature dependence of the photovoltage can be obtained from the expression for the current.

$$I = I_s - A_o T^2 e^{-\phi_b/KT} \left[ e^{qV/KT} - 1 \right] \quad (2.3.1)$$

The open circuit voltage,  $V_{oc}$ , is obtained by solving the above for  $V$  when  $I$  is set to zero.

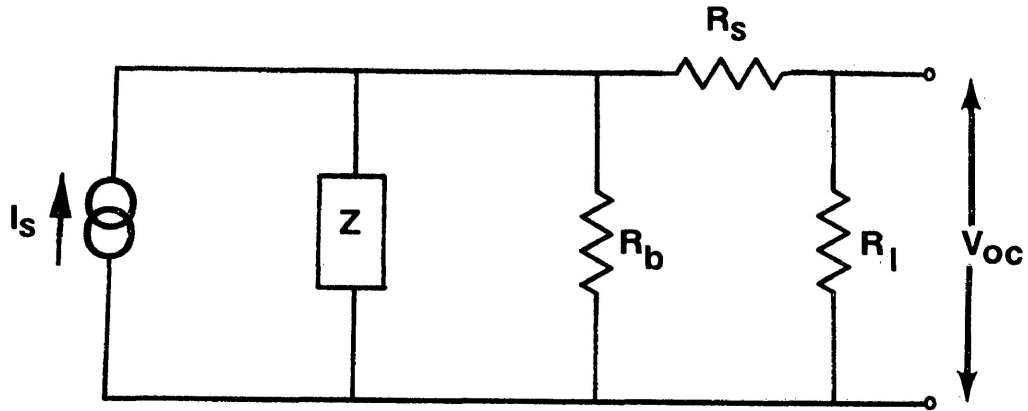


FIG. 5. Equivalent circuit of metal-semiconductor photovoltaic cell.

$I_s$  represents the illumination current,  $Z$  the barrier's nonlinear impedance,  $R_b$  a shunt resistance in the barrier responsible for leakages,  $R_s$  is the resistance of the cell bulk,  $R_l$  the external load resistance and  $V_{oc}$  the measured photovoltage.

$$V_{oc} = (KT/q)\ell n \left[ 1 + \frac{I_s e^{\phi_b/KT}}{A_o T^2} \right] \quad (2.3.2)$$

The thermal current from the semiconductor is proportional to  $e^{-E_g/KT}$  where  $E_g$  is the energy gap and the open circuit voltage decreases exponentially with an increase in temperature due to an increase in the dark current (1.4.3). Thus,  $V_{pv}$  is relatively large in large gap semiconductors at room temperature and conversely it tends to be small in a small-gap semiconductor.

The shunt resistance  $R_b$  is much greater than  $Z$  for high temperatures so that the current  $V/R_b$  passing through  $R_b$  is a small fraction of  $I_s$  and can be ignored. When this current becomes a significant factor, as it may at low temperature due to the exponential increase in  $Z$  with cooling, the open circuit voltage equation is no longer valid and must be modified. This can be done by adding a term  $V/R_b$  to the current expression (2.3.1) to account for this leakage effect.

$$I = I_s - A_o T^2 e^{-\phi_b/KT} \left[ e^{qV/KT} - 1 \right] - V/R_b \quad (2.3.3)$$

If the photovoltage is now obtained when  $I = 0$ , one has (after noting that  $C' = I_s/A_o$  and  $D = A_o R_b$ )

$$C' - V_{oc}/D = T^2 e^{-\phi_b/KT} \left[ e^{qV/KT} - 1 \right] \quad (2.3.4)$$

as the fit equation under these conditions. To obtain the open-circuit photovoltage predicted by this expression one can solve using iteration techniques.

#### 2.4 EXPERIMENTAL PROCEDURE

The temperature dependence of the photovoltage was obtained over the room temperature to 8°K range. As was already described, chopped light and lock-in techniques were employed. In some of the GaAs samples the a.c. measurements taken using the lock-in detector tended to decrease at low temperature. This was accompanied by a change in signal wave shape from that of a square wave to one consisting of rising and falling RC voltages. This was attributed to the increasing sample resistivity, and was avoided by switching to d.c. measurements. Fig. 6 illustrates the high and low temperature wave shapes and the different temperature-voltage curves obtained using a.c. and d.c. measurements.

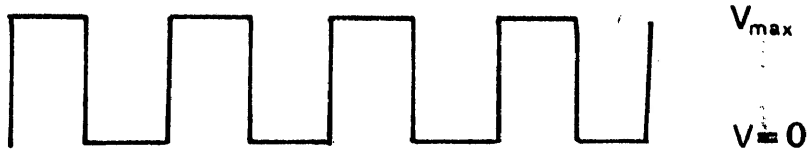


Fig. 6a) Waveform observed without RC effect.



Fig. 6b) Waveform observed with RC effect.

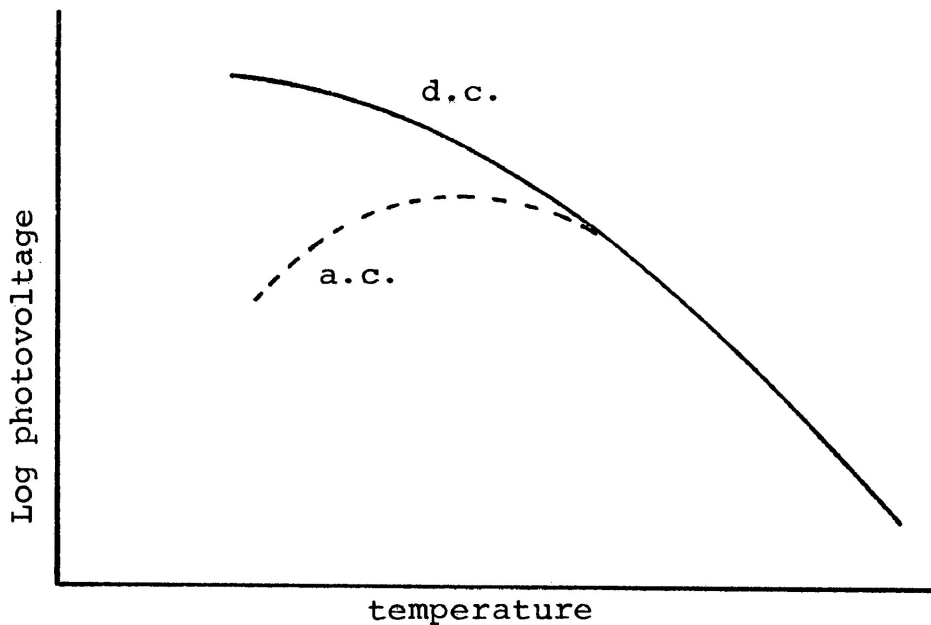


Fig. 6c) Photovoltage vs. temperature obtained from the d.c. and reduced a.c. measurements.

**FIG. 6.** PHOTOVOLTAGE OBTAINED WITH AND WITHOUT RC EFFECT IN BOTH THE d.c. AND a.c. MEASUREMENTS

The input impedance of a detector (oscilloscope, lock-in detector, etc.) may load the sample particularly at low temperature when the semiconductor resistivity is highest. This phenomenon was often observed when using the oscilloscope as a monitor device since its input impedance was only about 1 meg. The lock-in detector, on the other hand, had a much higher input impedance (1000 megs.) and therefore recorded the full signal strength provided time constant effects did not occur as outlined above. Experiments to test the effect of an even higher input impedance were attempted using a FET op-amp configured as a very high input impedance (greater than  $10^{15}$  ohms) preamp. The results, however, were not an improvement beyond those of the lock-in itself. In fact, this preamp had to be abandoned because, with such a high input impedance, sample charging began to occur due to photoemission of electrons from the sample, and an offset of up to 1.5 volts could be developed.

The photovoltages were usually recorded during both cooling and warming runs. Because of the refrigerator's thermal time constant characteristics, it was easier to obtain accurate data during a slow warming run. Thus, most of the results presented in this thesis are for warming runs.

## CHAPTER III - RESULTS AND DISCUSSION

### 3.1 GENERAL

The barrier values were obtained primarily using eq. (2.3.2) which appeared to fit experiment well for the higher temperature limit of each curve. The computer graphic plot routine is listed in the Appendix. To illustrate the general behaviour predicted by this expression, Fig. 7 shows the equation plotted for a range of  $\phi_b$  values with the constant  $C'$  held fixed at one for convenience.

The term  $\ln(1+x)$  comprises the major temperature dependent portion of the fit and can be thought of as having high and low temperature limits depending on the relative size of  $x$ . The higher temperature limit has  $x \ll 1$  so the approximation becomes  $x$  which is exponential in  $T$ . At low temperature we eventually find  $x > 1$  and the approximation changes to  $\ln x$  which is slowly varying with temperature. Samples whose results require a large  $\phi_b$  and/or large  $C'$  will behave as though they are in the low temperature limit, even at room temperature while small values of  $\phi_b$  lead to exponential variation with temperature, i.e., conform to the high temperature limit. Examples of the former will include GaAs and GaSb photocells while the various InSb samples will be examples of the latter case.

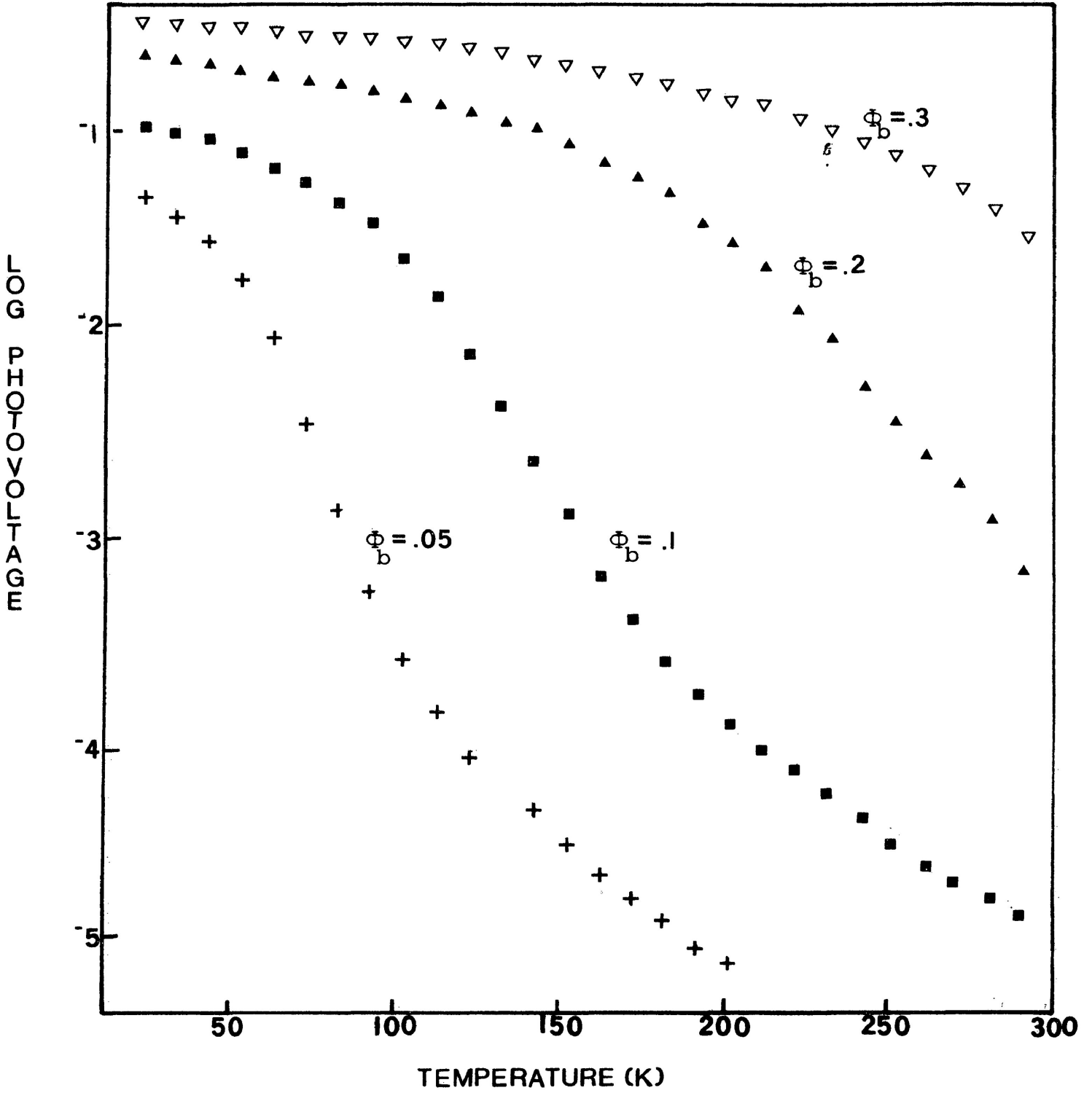


FIG. 7. Photovoltages generated using equation (2.3.2) for a range of  $\phi_b$  values with the constant  $C'$  held fixed.

Figure 8 shows the general dependence of the curves on variation in  $C'$  for a fixed value of  $\phi_b$ . In the results which follow, adjustments to these two parameters  $\phi_b$  and  $C'$ , were all that was used for fitting the "high temperature" portions of the curves. The experimental photovoltages generally fell below the predicted values at low temperature. Possible reasons for this will be investigated in section 3.3.

The reported values of the work function for gold (Au) and silver (Ag) are quite widely spread [20,21]. The ranges are listed in Table 1. The measured electron affinities for the semiconductors studied are also shown. These are more narrowly defined and have an average uncertainty of about 0.05 eV.

TABLE 1  
WORK FUNCTIONS AND ELECTRON AFFINITIES

	$\phi_m$ (eV)	$\chi_s$ (eV)	Value used (eV)
Au	4.7 - 5.2		4.80
Ag	4.2 - 4.4		4.30
InSb		4.59	4.60
GaAs		4.07	4.07
GaSb		4.06	4.06

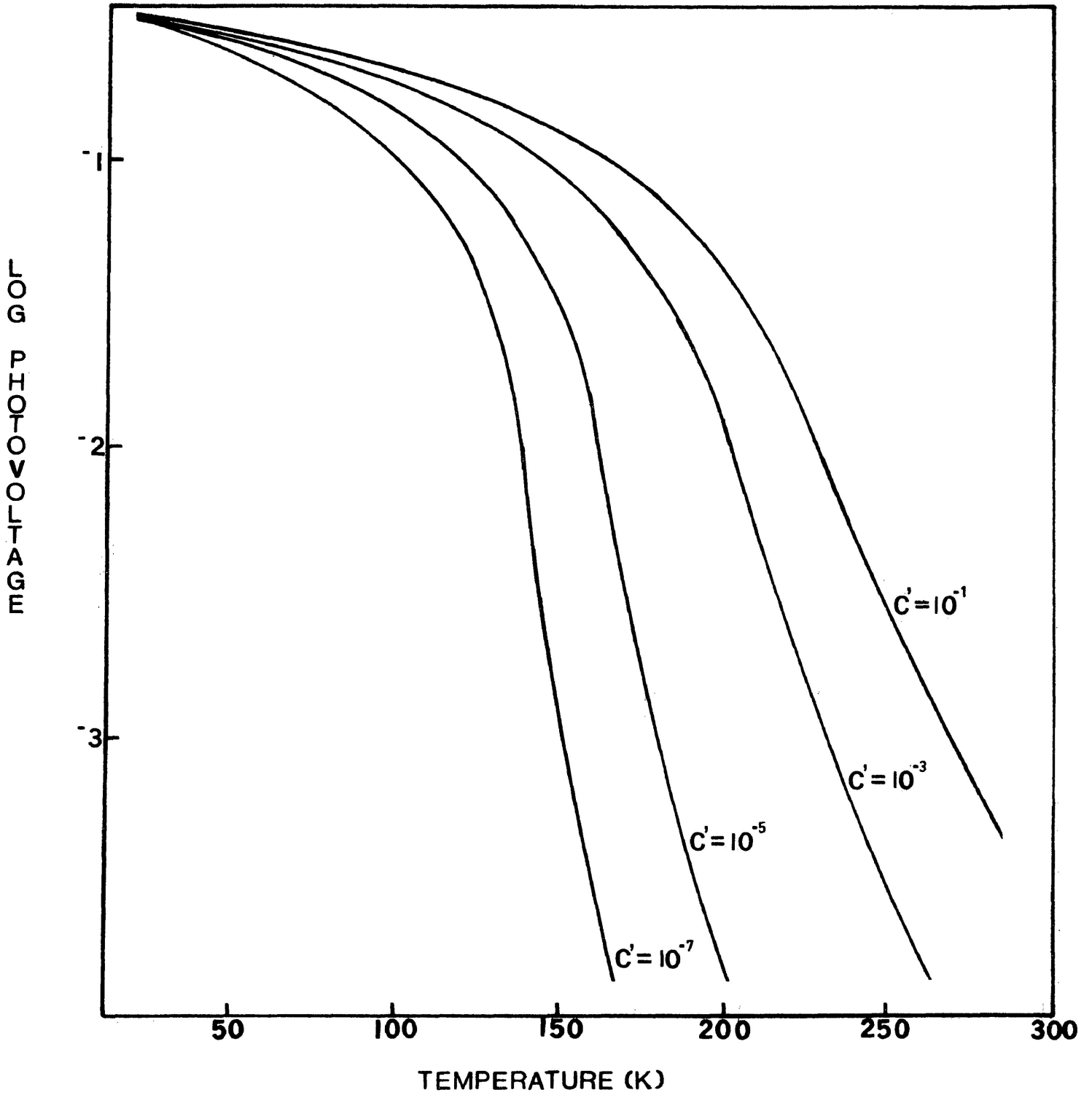


FIG. 8. The general dependence of the curves on variation in  $C'$  for a fixed value of  $\phi_b$  as predicted by equation (2.3.2).

### 3.2 EXPERIMENTAL RESULTS

#### (1) n-InSb:Ag

Figure 9 shows experimental results and the theoretical fit for one of the three samples tested. Taking  $\phi_m = 4.30$  eV as the best choice for the work function for silver, and noting that at high temperature (intrinsic limit) the work function for InSb should be approximately equal to the electron affinity  $X_s = 4.60$  eV, a barrier calculated from Fermi level differences would be

$$\begin{aligned}\phi_b &= |\phi_m - \phi_s| \\ &= (4.60 - 4.30)\text{eV} = 0.30 \text{ eV}.\end{aligned}$$

This is in good agreement with the best fit value of 0.29 eV. It is also interesting to note that  $\phi_b$  is almost twice the energy gap  $E_g$ .

#### (2) p-InSb:Ag

Figures 10 and 11 show experiment and theory for two different samples. There are several points of interest in the results for this combination. First of all, at high temperature the results are similar to those for the n-type sample. Since both are intrinsic above about 150<sup>o</sup>K,

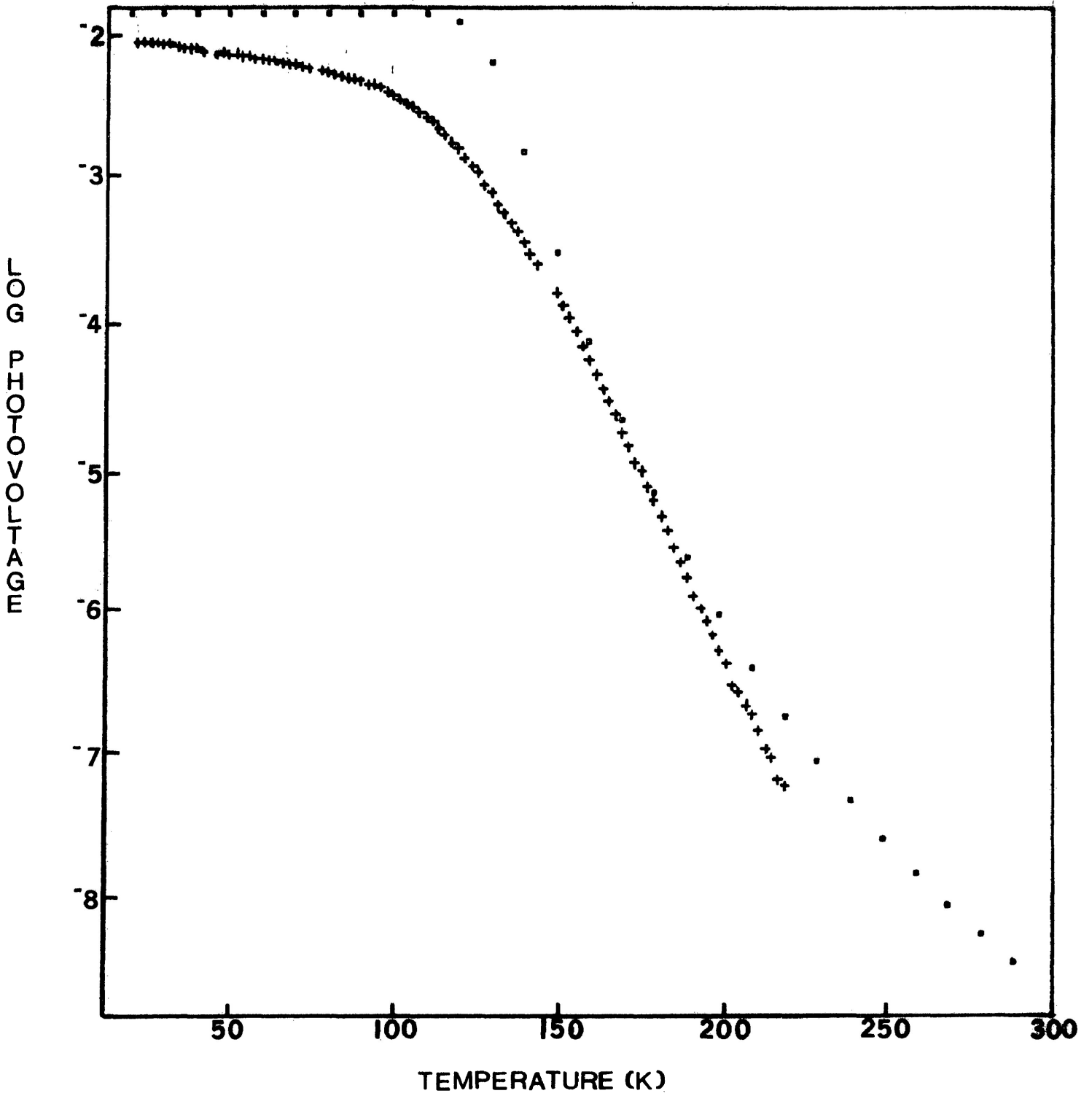


FIG. 9

n-InSb:Ag

• • • theoretical fit

\*\*\* experimental

$$\phi_b = 0.29 \text{ eV}$$

$$C' = 1 \times 10^{-7}$$

$$D = 140000$$

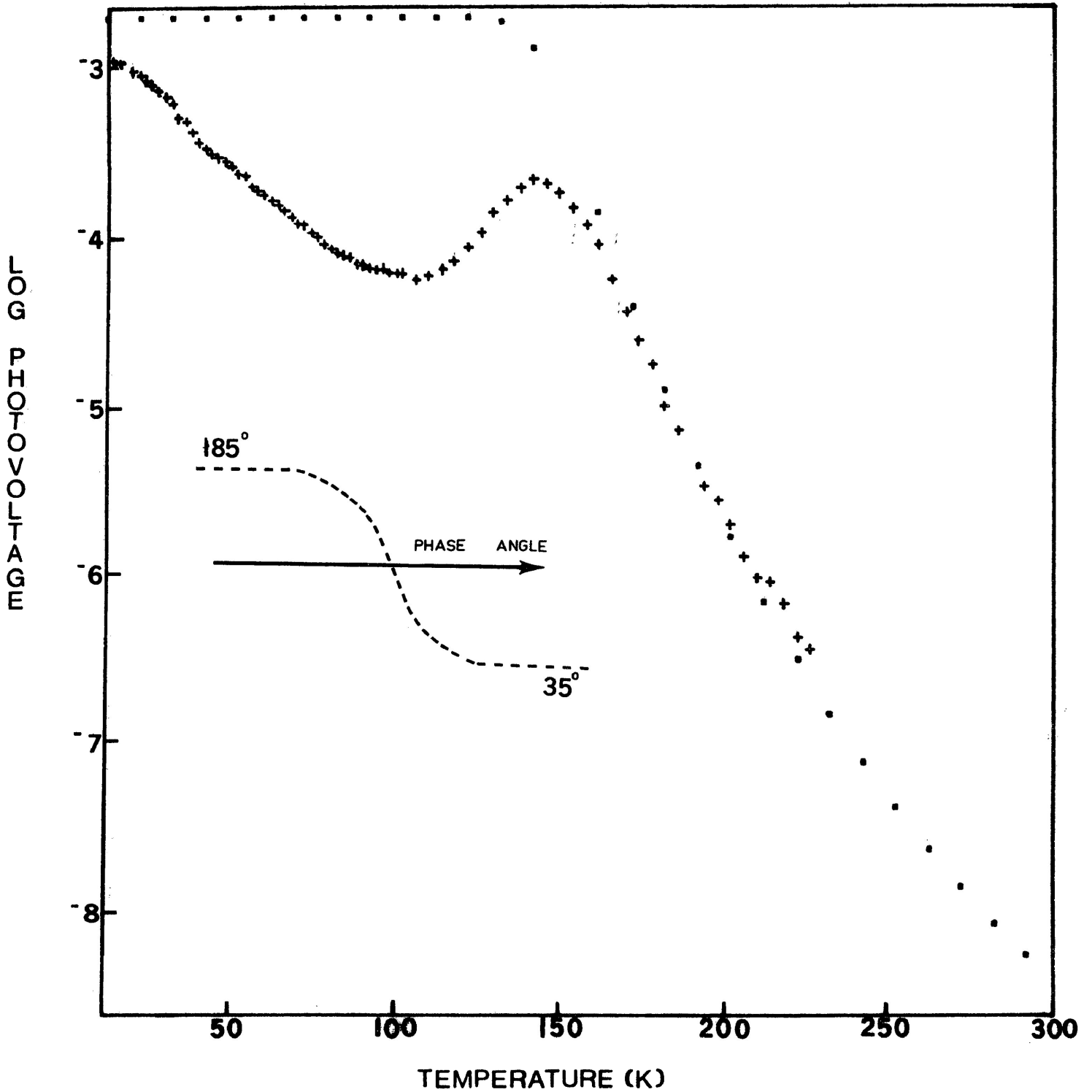


FIG. 10

p-InSb:Ag(1)

• • • theoretical fit

\*\*\* experimental

$$\phi_b = 0.3 \text{ eV}$$

$$C' = 1 \times 10^{-7}$$

$$D = 20000$$

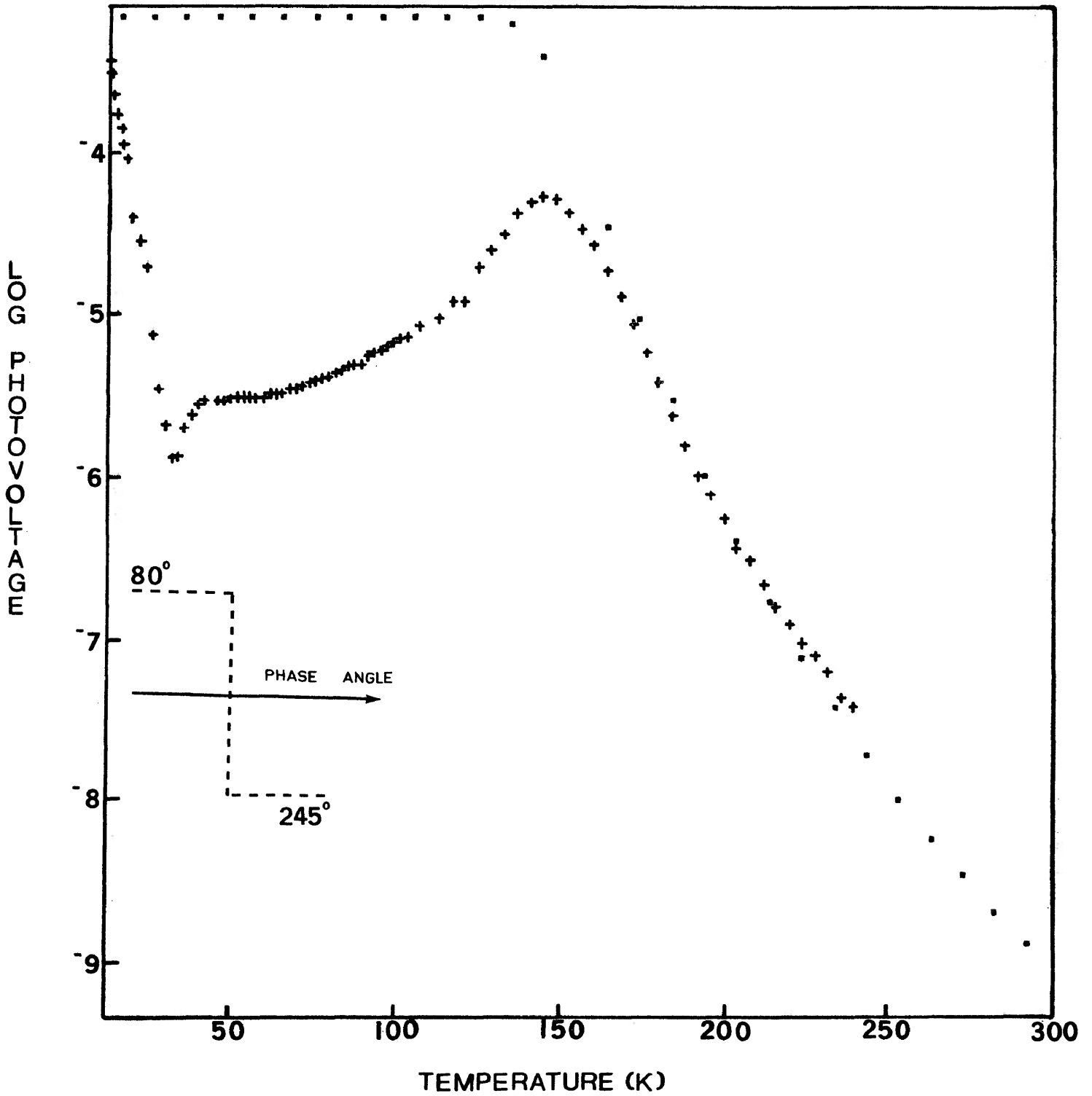


FIG. 11

p-InSb:Ag(2)

• • • theoretical fit

\*\*\*\* experimental

$$\phi_b = 0.3 \text{ eV}$$

$$C' = 2.4 \times 10^{-8}$$

$$D = 29170$$

their behaviour is apparently identical. The fact that the same barrier results in these cases can only be explained by assuming that the barrier is dependent on a difference in the positions of the Fermi levels in the metal and semiconductor. The Fermi level for the InSb is close to the conduction band when it is intrinsic because of the large effective mass ratio for holes to electrons. Taking  $E_f \approx X_s \approx 4.60$  eV and  $\phi_m = 4.30$  eV gives a difference of 0.30 eV which is very close to the best fit value. Since the barrier is greater than the energy gap  $E_g$ , the surface states model or any other which gives the barrier as some fraction of the gap  $E_g$  is effectively ruled out.

A second point of interest is the reduction in the photovoltage as the material begins to turn extrinsic near 150°K. As the Fermi level in the semiconductor falls towards the valence band, the barrier height should increase if one uses a simple Fermi level difference argument. However, at the same time the dominant carrier type is also changing as is evident from the phase change of almost 180 degrees in the photovoltage. Thus an effect somewhat similar to the Hall process must be present where the photovoltage is determined by a difference in products  $\mu_p p$  and  $\mu_n n$  and not just the n/p ratio. Because the change in phase is spread

out over different temperature ranges in the two samples, one concludes that different carrier mobilities associated with different metal film depositions on the two samples, are playing a role in reversing the sign of the photovoltage.

Some authors [20,22] would argue that this system should be ohmic because  $\phi_m$  lies higher in energy than  $\phi_s$  and there are empty semiconduction band states available to the metal electrons. Clearly this does not appear to matter and a barrier is apparently formed because of the charge transfer which occurs when the Fermi levels align.

### 3. n-InSb:Au

Figure 12 shows the experimental data and best fit curve at both high and low temperature. Taking the work function of Au as 4.80 eV and that of intrinsic InSb as 4.60 eV, the barrier height  $\phi_b$  should be given by (since  $\phi_s = X_s$ )

$$\begin{aligned}\phi_b &= \phi_m - \phi_s \\ &= 0.20 \text{ eV}\end{aligned}$$

At high temperature, eq. (2.3.2) was used for the fit. The best fit for the barrier height is obtained as 0.178 eV

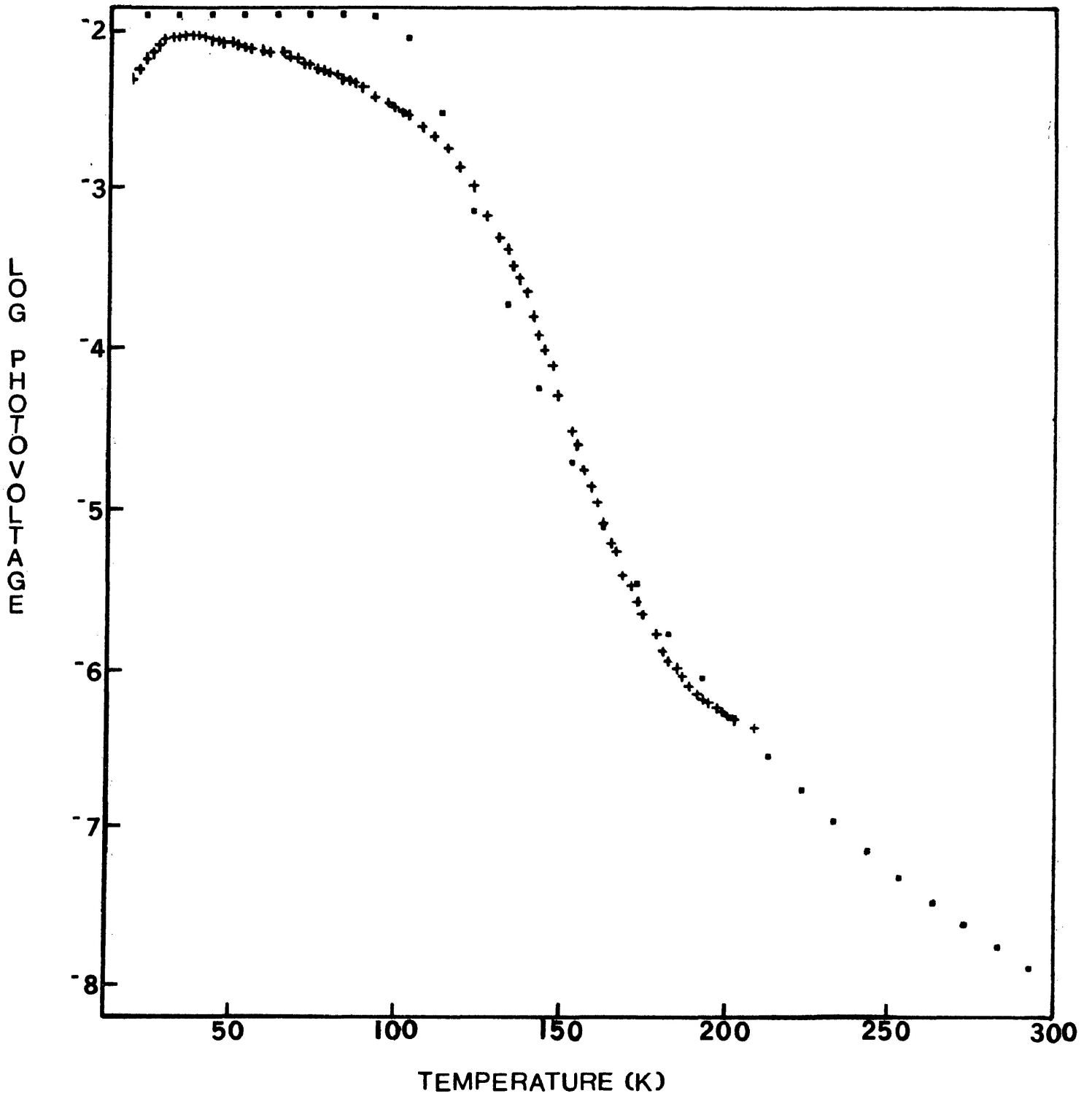


FIG. 12

n-InSb: Au

. . . theoretical fit

\*\*\* experimental

$$\phi_b = 0.178 \text{ eV}$$

$$C' = 3.7 \times 10^{-5}$$

$$D = 351.4$$

and the constant  $C' = 3.7 \times 10^{-5}$ . The photovoltage does not limit to  $\phi_b/q$  at absolute zero. If the low temperature region is assumed to have a leakage loss, eq. (2.3.4) can be used. When this was done, the same barrier and  $C'$  value are retained but  $D$  was found to be 351.4. The barrier height obtained from C-V analysis is found to be about 0.17 eV in good agreement with the present result.

(4) p-InSb:Au

In this sample no significant photosignal was observable until the temperature was lowered to about 180°K as illustrated in Fig. 13. Thus as the signal is increasing, the semiconductor is entering the extrinsic phase. This should lead to the semiconductor Fermi energy being approximately  $X_s + E_g$  or about 4.78 eV. Since this is also the approximate size of the gold work function, one expects a very small barrier. The best fit value of 0.059 eV supports this prediction.

(5) n-GaAs:Au

Figure 14 shows the best fit results are obtained when  $\phi_b = 0.73$  eV and the value of  $C' = 0.0044$ . Again taking  $\phi_m$  as 4.80 eV for gold and  $\phi_s$  as the n-type extrinsic value

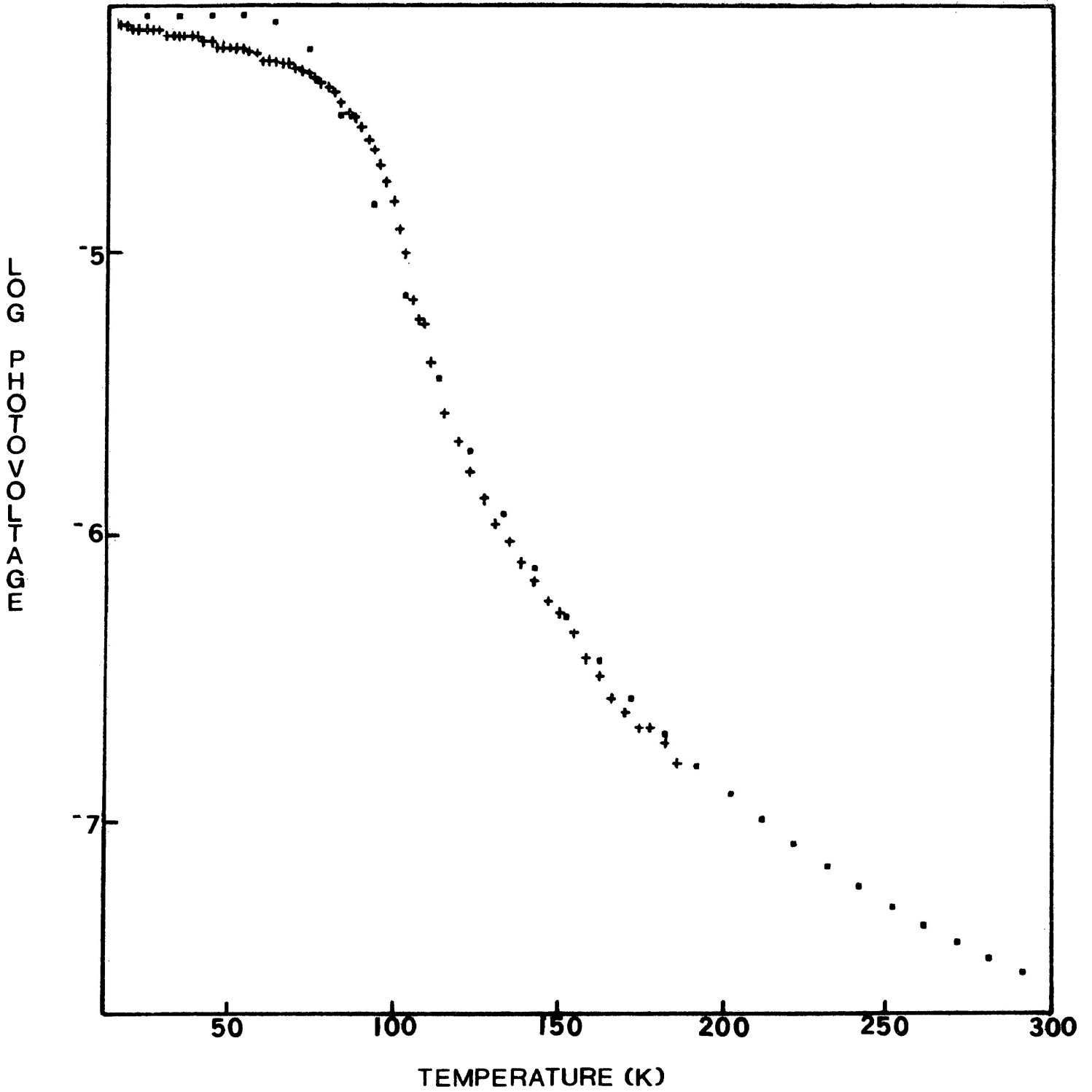


FIG. 13

p-InSb-Au

. . . theoretical fit

\*\*\*\* experimental

$$\phi_b = 0.059 \text{ eV}$$

$$C' = 0.01$$

$$D = 0.007$$

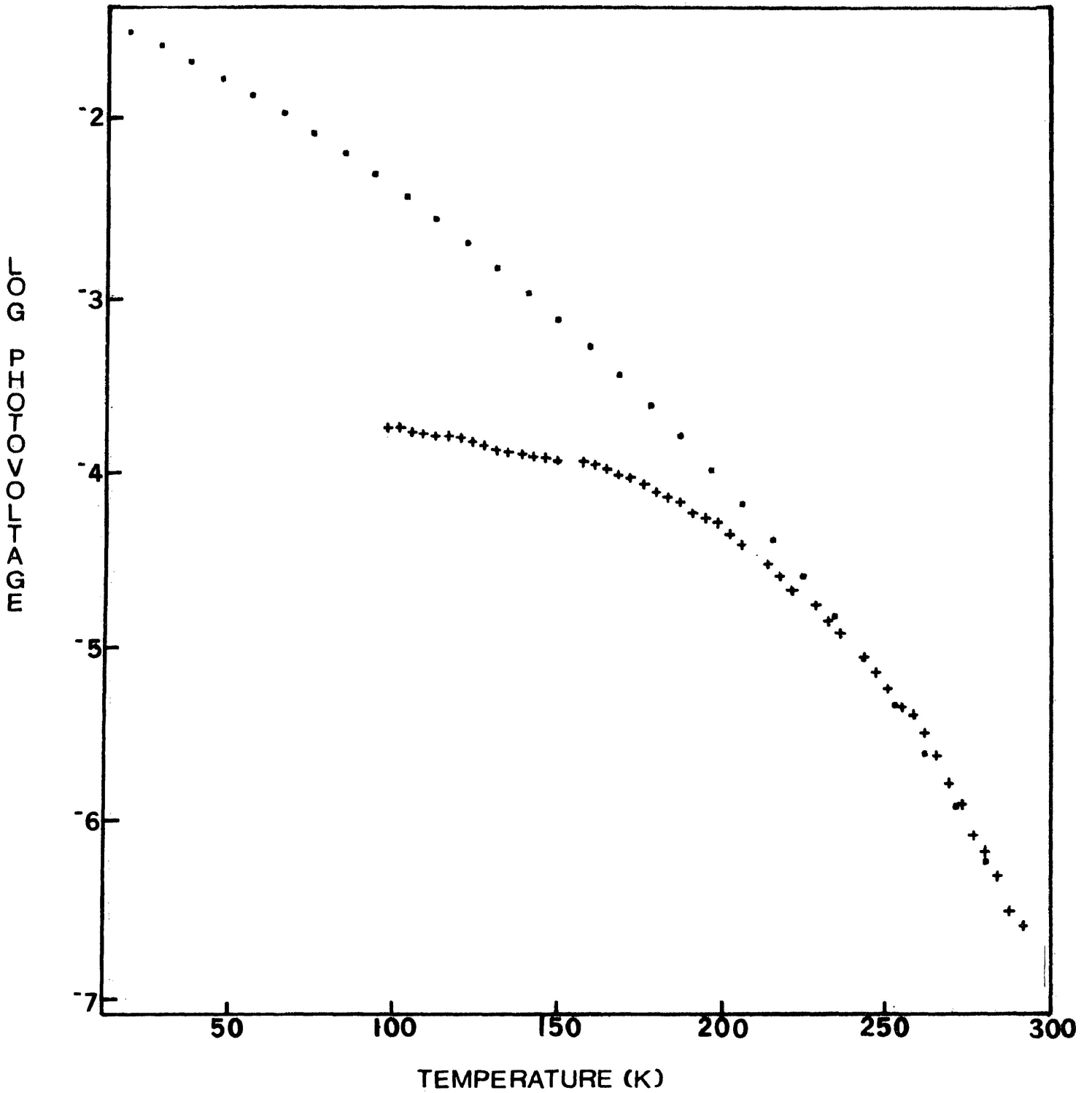


FIG. 14

n-GaAs:Au

• • • theoretical fit

\*\*\*\* experimental

$$\phi_b = 0.73 \text{ eV}$$

$$C' = 4.4 \times 10^{-4}$$

of approximately  $X_s = 4.07$  eV for GaAs, one expects  $\phi_b$  of about 0.73 eV. This value is fortuitously close to that measured. Note earlier experimental values of about 0.9 eV have been claimed.

For the GaAs samples in particular, we noted a tendency to long time-constants and hence a slow rise and fall in the photosignal as the light was chopped. This is undoubtedly due to its large gap and hence high sample resistivity. To make sure the total signal swing was being measured, we had to slow down the chopper rate and/or resort to a d.c. measurement of the photosignal to obtain the full amplitude.

(6) n-GaAs:Ag

The best fit results are  $\phi_b = 0.30$  eV and  $C' = 1.4$  as shown in Fig. 15. Assuming the value of  $\phi_m = 4.30$  eV and  $\phi_s = 4.07$  eV the barrier is predicted to be about 0.23 eV. While lower than observed, the agreement still lies well within the uncertainty limits on the work function and electron affinities used.

Both the GaAs and GaSb cells have small thermal current contributions because of their relatively large energy gaps. Thus the photocurrent to thermal current ratio

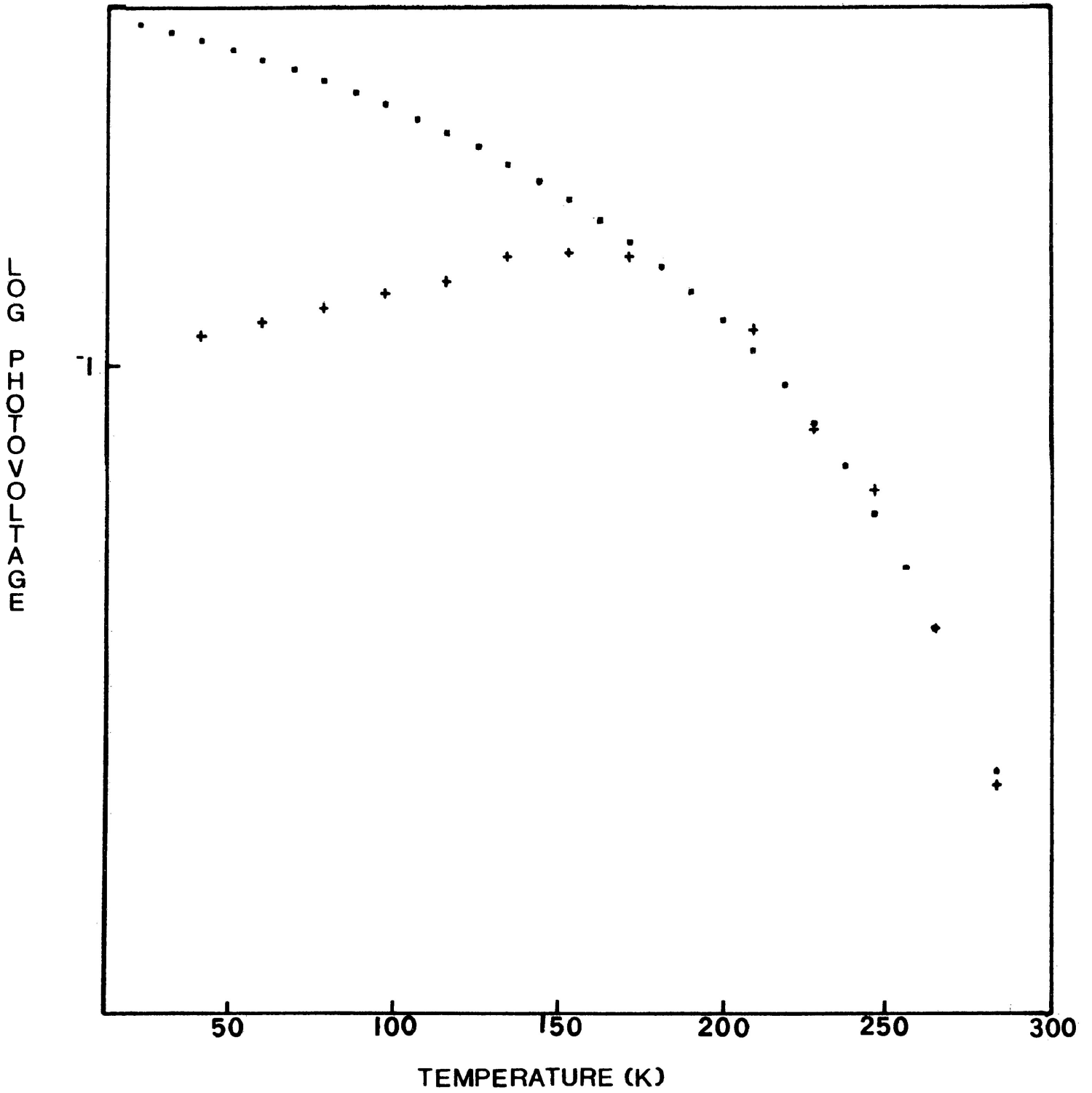


FIG. 15  
n-GaAs:Ag

• • • theoretical fit  
 $\phi_b = 0.3$  eV  
 $C' = 1.6$

++++ experimental

is large leading to apparent "low temperature limit" behaviour even at room temperature.

(7) n-GaSb:Ag

Analysis of the result gives a barrier height of 0.225 eV and  $C'$  is 3.0 as in Fig. 16. Taking the value of  $\phi_m = 4.30$  eV and  $\phi_s = 4.06$  eV results in a Fermi level difference barrier height prediction of 0.24 eV.

(8) We also tried to produce photovoltages using n and p-InAs with Au but obtained only ohmic contacts. This semiconductor has an unusually large electron affinity  $X_s = 5.2$  eV which might have something to do with the result. Also, the material was quite low in resistivity (i.e., high impurity content) which would favour ohmic contacting. Further studies on InAs will await the arrival of high purity material.

### 3.3 LOW TEMPERATURE EFFECTS

It is clear from the fits that eq. (2.3.2) appears to give a good method of obtaining a barrier from the high

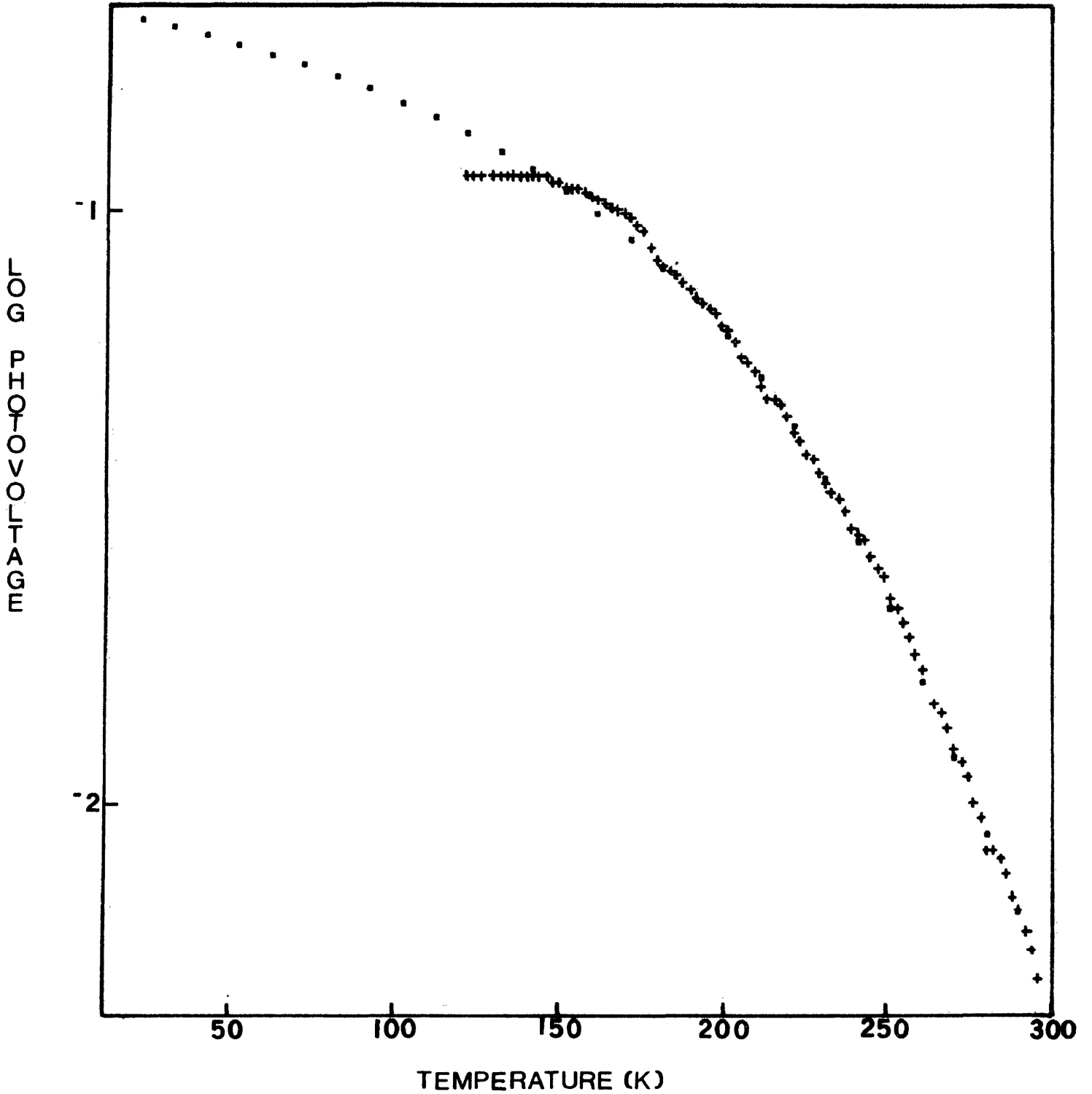


FIG. 16  
n-GaSb:Ag

• • • theoretical fit      +++ experimental  
 $\phi_b = 0.225 \text{ eV}$   
 $C' = 3.0$

temperature portion of each of the curves. The agreement at low temperature while correct in trend, is not absolute.

The general tendency for the experimental photovoltage results to fall below the prediction in eq. (2.3.2) at low temperature is not completely understood. Some of the possible mechanisms which could lead to this behaviour include (i) shorts through the barrier region, (ii) a tunnelling contribution to the competing current densities, (iii) a temperature dependent recombination rate for optically created carriers and (iv) lateral photovoltage effects.

From the equivalent circuit analysis, surface leakage around the junction, along edges or along grain boundaries, or shorts through the junction itself, would reduce the signal available for external use. This could be represented as an equivalent conductance shunting the photosource. As the sample is cooled, the source impedance  $Z$  increases. When it becomes comparable in magnitude to the leakage shunt conductance  $1/R_b$ , a growing portion of the total current  $I_s$  will begin to flow through this additional path and a reduced photovoltage results. If this conductance is assumed to be temperature independent,

at low temperature the photovoltage should become a constant equal to  $I_s \times R_b$ .

Padovani et al. [23] and C.R. Crowell et al. [24] have predicted that tunnelling could lead to a reduced photovoltage at low temperature. We have not tried to quantify this as there are too many assumptions required.

There is some evidence to suggest that there might be a temperature dependence to any recombination contribution to the total current densities. Hovel [25] argues that the total dark current expression in the diode equation is the sum of the injection current,  $I_{inj} e^{qV/KT}$  and a recombination current  $I_{rg} e^{qV/2KT}$ . The high temperature sum is then dominated by the injection current, while the recombination current becomes increasingly important at low temperature. If the latter becomes dominant, the photovoltage would show a temperature dependence at low temperature due in part to this effect. Since the measured low temperature results appear to be mainly shifted, with no change in temperature dependence from that of eq. (2.3.4) it does not seem that a temperature dependent recombination process is operating.

A process called the "lateral photo effect" is described by Alferov et al. [26]. This effect produces

a maximum in the photovoltage when the light is shone on the edge of the photocell instead of the centre. We observed signal amplitude variation as a function of light beam positioning in almost all the samples studied and the amplitude was usually largest when the cell was partly edge illuminated. When samples were run with different light beam positioning, the resulting curves appeared offset by a constant amount on a semilog plot. Thus, this effect does not change slopes in  $V$  vs.  $T$  plots but does produce absolute shifts which then lead to disagreement with eq. (2.3.2) at low temperature.

Because of the many processes which can affect the absolute low temperature voltage, it becomes impossible to quantify or suggest a single most likely correction term to be added at low temperature. Nonetheless, the high temperature region of each curve seems to allow quite sensitive extraction of a barrier value for all the samples reported here.

CHAPTER IV - CONCLUSION

The temperature dependence of the photovoltaic effect has been used to obtain the Schottky barrier heights for some of the III-V semiconductors with Au and Ag. The method appears to be quite sensitive and works particularly well for barriers below about 0.5 eV, although the method still works up to about 0.7 eV. The semiconductors investigated were GaAs, GaSb and InSb with energy gaps of 1.4 eV, 0.7 eV and 0.18 eV, respectively. The photovoltage produced when light shines on the cell increases when the ratio of the photocurrent to the thermal current decreases. Since the thermal current decreases for large gap semiconductors, these tend to produce the largest photovoltages even if the barrier is small. This can be seen clearly from the experimental results.

Table 2 contains a listing of the barriers obtained for the various photocells and compares them to previously obtained values.

TABLE 2

RESULTS

Semiconductor	Metal	C-V Experimental (eV) [27]	Difference in Fermi levels (eV)	Photo- voltage expt. (eV)
n-InSb	Au	0.17±0.01	0.20±0.10	0.178
n-InSb	Ag	0.18	0.30±0.10	0.29
p-InSb	Ag (1)		0.30±0.10	0.30
p-InSb	Ag (2)		0.30±0.10	0.30
p-InSb	Au	ohmic	0.03±0.10	0.059
n-GaAs	Au	0.95±0.03	0.73±0.10	0.73
n-GaAs	Ag	0.93±0.03	0.22±0.10	0.30
n-GaSb	Ag		0.24±0.10	0.225

The above results suggest that the barrier height is reasonably predicted by taking the difference in the Fermi energy of the metal and semiconductor. The barriers obtained for both the n and p type InSb with silver samples are larger than the energy gap of InSb. This result cannot be explained using a surface states argument or the "two-thirds  $E_g$ " rule [27].

At low temperatures the measured photovoltages fall below the value predicted by eq. (2.3.2). This decreased photosignal is still not understood but may be due to the effects as outlined in Section 3.3.

The rather large uncertainty assigned to the difference in Fermi levels in Table 2 is an attempt to accommodate the variation in reported experimental work functions. The variation in the values for gold and silver in particular were much larger than the quoted experimental uncertainty by any individual reporting group. However, the values chosen (and reported in Table 1) appear to provide a difference which is in very good agreement with the photovoltage barrier for all samples investigated.

REFERENCES

1. P. Rochon, E. Fortin and J.C. Woolley, Can. J. Phys. 55, 1145 (1977).
2. W.J. Keeler, A.P. Roth and E. Fortin, Can. J. Phys. 58, 560 (1980).
3. A.P. Roth, W.J. Keeler and E. Fortin, Can. J. Phys. 58, 63 (1980).
4. H.K. Henisch, Rectifying Semiconductor Contacts, Oxford at the Clarendon Press, Oxford (1957).
5. A.M. Cowley and S.M. Sze, J. Appl. Phys. 36, 3212 (1965).
6. J.I. Pankove, Optical Process in Semiconductors, p. 312, Prentice-Hall, Englewood Cliff, N.J. (1971).
7. G. Louie and M.L. Cohen, Phy. Rev. B13, 2461 (1976).
8. J.R. Chelikowsky, Phy. Rev. B16, 3618 (1977).
9. C.A. Mead, Solid State Electronic Vol. 9, pp 1023-1033 (1966).
10. R. Crowell, Solid State Electronic Vol. 8, 395 (1965).
11. S.M. Sze, Physics of Semiconductor Devices, Ch. 8, Willey, New York, N.Y. (1969).
12. J.I. Pankove, Optical Process in Semiconductors, p. 303, Prentice-Hall, Englewood Cliff, N.J. (1971).
13. L.D. Hunter, Introduction to Semiconductor Phenomena and Devices, Ch. 4, Addison-Wesley, Reading, Mass. (1966).

14. L.V. Azaroff and J.J. Brophy, Electronic Process in Materials, p. 311, McGraw-Hill, New York, N.Y. (1963).
15. M. Neuberger, Handbook of Electronic Materials 2, Plenum, New York, N.Y. (1971).
16. B.L. Sharma, Diffusion in Semiconductors, Trans Tech Publication, Germany (1970).
17. J.J. Loferski and P. Rappaport, Methods of Experimental Physics 6B, 365 Academic Press, New York (1959).
18. R.H. Bube, Photoconductivity of Solids, John Wiley, New York, N.Y. (1960).
19. Rafik O. Loutfy and Cheng-Kao Hsiao, Can. J. Phys. 59, 727 (1981).
20. A.G. Milnes and D.L. Feucht, Heterojunctions and Metal Semiconductor Junctions, Ch. 6, Academic Press, New York (1972).
21. R.K. Willardson and A.C. Beer, Semiconductors and Semimetals, Vol. 2, p. 275, Academic Press Inc., N.Y. (1966).
22. Van der Ziel, Solid State Physical Electronics 2nd Ed. Prentice-Hall Inc., Englewood Cliffs, New Jersey (1968).
23. F.A. Padovani and R. Stratton, Solid State Electronics 12, 695 (1966).
24. C.R. Crowell and V.L. Rideout, Solid State Electronics 12, 89 (1966).
25. H.J. Hovel, Semiconductors and Semimetals, Vol. 11, Ch. 3, Academic Press Inc., N.Y. (1975).

26. J.I. Alferov, V.M. Andreev, E.L. Portnoi and I.I. Protasov, Sov. Phys. Semiconductors 3, 1103 (1970).
27. C.A. Mead and Spitzer, Physical Review, 134, A173 (1964).

APPENDIX

```
10 REM *****
20 REM * This Program Calculates and Plots Photovoltages for *
30 REM * any temperature using eq.(1.4.5). Experimental data *
40 REM * is also displayed. *
50 REM * The Program is written in Microsoft Basic for a North *
60 REM * Star Horizon Computer. The Printer used was an *
70 REM * Anadex 9501 graphics unit. August 1982. *
80 REM *****
90 REM
100 REM ;;;;;;;;;;;;;;;;;;;;;;;;;;;;;;;;;;;;;;;;;;;;;;;;;;;;;;;;;;;;;;;;;;
110 REM ; This module reads a data file from a disk
120 REM ;;;;;;;;;;;;;;;;;;;;;;;;;;;;;;;;;;;;;;;;;;;;;;;;;;;;;;;;;;;;;;;;;;
130 REM
140 DIM T(100),V(100) :REM Horiz. and vertical data vectors.
150 INPUT "READ EXISTING FILE FROM DISK";NO$
160 IF STRING$(1,NO$)="N" GOTO 230
170 INPUT "FILE NAME IS ";A$ :REM Input data from disk file.
180 OPEN "I",#1,A$
190 IF EOF(1) THEN GOTO 230
200 INPUT#1,R,T(R),V(R)
210 V(R)=V(R)*2.83/1000
220 PRINT R,T(R),V(R) :R=R+1 :GOTO 190
230 INPUT "INPUT DATA";NO$ :REM Input add. data from keyboard?
240 IF STRING$(1,NO$)="N" GOTO 290
250 INPUT "LOCATION";R
260 INPUT "TEMP";T(R)
270 INPUT "VOLTS";V(R)
280 GOTO 230
290 R=R-2
300 REM
310 REM ;;;;;;;;;;;;;;;;;;;;;;;;;;;;;;;;;;;;;;;;;;;;;;;;;;;;;;;;;;;;;;;;;;
320 REM ; The character string below is the vertical axis label.
330 REM ;;;;;;;;;;;;;;;;;;;;;;;;;;;;;;;;;;;;;;;;;;;;;;;;;;;;;;;;;;;;;;;;;;
340 REM
350 DIM TC(100),VC(100),C$(50),TE(100),VE(100)
360 C$(28)="L":C$(27)="O":C$(26)="G"
370 C$(24)="P":C$(23)="H":C$(22)="O":C$(21)="T":C$(20)="O":C$(19)="V"
380 C$(18)="O":C$(17)="L":C$(16)="T":C$(15)="A":C$(14)="G":C$(13)="E"
390 REM
400 REM ;;;;;;;;;;;;;;;;;;;;;;;;;;;;;;;;;;;;;;;;;;;;;;;;;;;;;;;;;;;;;;;;;;
410 REM ; This section calculates theoretical photovoltages.
420 REM ;;;;;;;;;;;;;;;;;;;;;;;;;;;;;;;;;;;;;;;;;;;;;;;;;;;;;;;;;;;;;;;;;;
430 REM
440 FOR I=1 TO R:V(I)=LOG(V(I))/2.303:NEXT
450 NO=30 :REM Find calculated points.
460 INPUT "Const and barrier";C,E
470 FOR I=1 TO NO :REM Input fit parameters in line above.
480 TC(I)=I*10 :REM Lines from NO to E1 can be replaced
490 E1=E/.0000862/TC(I) :REM and any other function calculated.
500 IF E1>60 THEN 560
510 IF C*EXP(E1)/TC(I)^2<.000001 THEN 540
520 VC(I)=.000086*TC(I)*LOG(1+C*EXP(E1)/TC(I))/TC(I)^2
530 GOTO 570
540 VC(I)=.0000862*C*EXP(E1)/TC(I)
550 GOTO 570
```

```
560 VC(I)=B+LOG(C)*.0000862*TC(I)-2*LOG(TC(I))*0.0000862*TC(I)
570 VC(I)=LOG(VC(I))/2.303:NEXT
580 B1=B
590 REM
600 REM ;;;;;;;;;;;;;;;;;;;;;;;;;;;;;;;;;;;;;;;;;;;;;;;;;;;;;;;;;;;;;;;;;;
610 REM ; This section sorts for min and max values of V and T.
620 REM ;;;;;;;;;;;;;;;;;;;;;;;;;;;;;;;;;;;;;;;;;;;;;;;;;;;;;;;;;;;;;;;;;;
630 REM
640 T1=T(1):T2=T(1):V1=V(1):V2=V(1)
650 FOR I=2 TO R :REM Find largest and smallest T value.
660 IF V(I)<V1 THEN V1=V(I)
670 IF V(I)>V2 THEN V2=V(I)
680 IF T(I)<T1 THEN T1=T(I)
690 IF T(I)>T2 THEN T2=T(I)
700 NEXT
710 FOR I=1 TO NO :REM Find largest and smallest V value.
720 IF TC(I)<T1 THEN T1=TC(I)
730 IF TC(I)>T2 THEN T2=TC(I)
740 IF VC(I)<V1 THEN V1=VC(I)
750 IF VC(I)>V2 THEN V2=VC(I)
760 NEXT I
770 REM
780 REM ;;;;;;;;;;;;;;;;;;;;;;;;;;;;;;;;;;;;;;;;;;;;;;;;;;;;;;;;;;;;;;;;;;
790 REM ; This section calculates horiz. and vert. axis decades
800 REM ;;;;;;;;;;;;;;;;;;;;;;;;;;;;;;;;;;;;;;;;;;;;;;;;;;;;;;;;;;;;;;;;;;
810 REM
820 A=T2-T1:B=V2-V1 :REM Horizontal and vertical range.
830 FOR N=0 TO 5:D=10^N :REM Find power of 10 in scales.
840 IF INT(A/D)=0 THEN GOTO 860
850 NEXT
860 D1=D/10 :REM D1 is horiz. factor of 1,10,100,..
870 FOR N=0 TO 5:D=10^N
880 IF INT(B/D)=0 THEN GOTO 900
890 NEXT
900 D2=D/10 :REM D2 is vertical factor.
910 REM
920 REM ;;;;;;;;;;;;;;;;;;;;;;;;;;;;;;;;;;;;;;;;;;;;;;;;;;;;;;;;;;;;;;;;;;
930 REM ; This section scales the points to be plotted.
940 REM ;;;;;;;;;;;;;;;;;;;;;;;;;;;;;;;;;;;;;;;;;;;;;;;;;;;;;;;;;;;;;;;;;;
950 REM
960 FOR I=1 TO R :REM Round off scaled T and V values to
970 :REM to nearest integer.
980 D=(T(I)-T1)*L1*N3/A:TE(I)=INT(D):IF D-TE(I)>.5 THEN TE(I)=TE(I)+1
990 D=(V(I)-V1)*L2*N4/B:VE(I)=INT(D):IF D-VE(I)>.5 THEN VE(I)=VE(I)+1
1000 NEXT
1010 FOR I=1 TO NO :REM Repeat for calculated points.
1020 D=(TC(I)-T1)*L1*N3/A:TC(I)=INT(D):IF D-TC(I)>.5 THEN TC(I)=TC(I)+1
1030 D=(VC(I)-V1)*L2*N4/B:VC(I)=INT(D):IF D-VC(I)>.5 THEN VC(I)=VC(I)+1
1040 NEXT
1050 REM
1060 REM ;;;;;;;;;;;;;;;;;;;;;;;;;;;;;;;;;;;;;;;;;;;;;;;;;;;;;;;;;;;;;;;;;;
1070 REM ; This section sets up the printer format.
1080 REM ;;;;;;;;;;;;;;;;;;;;;;;;;;;;;;;;;;;;;;;;;;;;;;;;;;;;;;;;;;;;;;;;;;
1090 REM
1100 N3=80:N4=40 :REM No's of rows and columns
```

```

1110 L1=6:L2=12 :REM Horiz. and vert. dots per char.
1120 M=INT(LOG(D2)/2.3)+5 :REM M is column pos. of left axis.
1130 LPRINT CHR$(25); :REM Set to 12.5 characters per inch.
1140 ML$=MID$(STR$(M*L1+1000),3) :REM ML$ is position of left margin.
1150 :REM expressed as a char string!
1160 MR$=MID$(STR$((M+N3)*L1+1000),3)
1170 IF A/D1<3 THEN D1=D1/2 :REM Divide by 2 if less than 3 temps.
1180 REM
1190 REM ;;;;;;;;;;;;;;;;;;;;;;;;;;;;;;;;;;;;;;;;;;;;;;;;;;;;;;;;;;;;;;;;;;
1200 REM ; This section prints graph one line at a time.
1210 REM ;;;;;;;;;;;;;;;;;;;;;;;;;;;;;;;;;;;;;;;;;;;;;;;;;;;;;;;;;;;;;;;;;;
1220 REM
1230 REM Next three program lines print top margin of graph.
1240 REM CHR$(28) enters printer graphics mode and CHR$(29) exits.
1250 REM
1260 LPRINT CHR$(28);"0;" + ML$;
1270 FOR I=1 TO N3*L1:LPRINT CHR$(96);:NEXT
1280 LPRINT CHR$(29);
1290 REM
1300 FOR N=N4 TO 0 STEP -1 :REM N is line no., 0 at page bottom.
1310 REM
1320 REM ;;;;;;;;;;;;;;;;;;;;;;;;;;;;;;;;;;;;;;;;;;;;;;;;;;;;;;;;;;;;;;;;;;
1330 REM ; This subsection prints the vert. axis title, the vert.
1340 REM ; axis and the voltage decade nos., but not points.
1350 REM ;;;;;;;;;;;;;;;;;;;;;;;;;;;;;;;;;;;;;;;;;;;;;;;;;;;;;;;;;;;;;;;;;;
1360 REM
1370 LPRINT C$(N); :REM C$ is vertical axis label.
1380 FOR J=2 TO 1 STEP -1 :REM J divides steps into half lines.
1390 V=(N+J/2-1/2)*B/N4+V1+.001 :REM V is line number in voltage units.
1400 IF V-D2*INT(V/D2)<B/N4/2 THEN LPRINT " ";INT(V/D2)*D2;
1410 REM
1420 REM The next two program lines close alphanumeric print record
1430 REM so that graphics mode can be reentered.
1440 REM
1450 LPRINT CHR$(13);
1460 LPRINT CHR$(28);
1470 P$=";" + ML$ + CHR$(127) + "0;" + MR$ + CHR$(127) :REM Print margins.
1480 REM
1490 REM ;;;;;;;;;;;;;;;;;;;;;;;;;;;;;;;;;;;;;;;;;;;;;;;;;;;;;;;;;;;;;;;;;;
1500 REM ; This subsection prints the points to high resolution.
1510 REM ;;;;;;;;;;;;;;;;;;;;;;;;;;;;;;;;;;;;;;;;;;;;;;;;;;;;;;;;;;;;;;;;;;
1520 REM
1530 FOR K=L2/2 TO 1 STEP -1 :REM There are 6 dots per half line.
1540 L=L2*N+L2/2*J+K-L2-1 :REM L is dot position on scaled V.
1550 V=L*B/N4/L2+V1
1560 IF V-D2*INT(V/D2)<B/N4/L2 THEN P$ =P$+"0;" + ML$ + "*****"
1570 FOR I=1 TO R :REM Search VE for any on current line.
1580 IF L-VE(I)<>2 GOTO 1610 :REM Ignore all points that aren't.
1590 M$=MID$(STR$(998+M*L1+TE(I)),3) :REM M$ is inset for data point.
1600 P$=P$+"0;" + M$ + "HH^HH" :REM Print a cross for data point.
1610 NEXT I
1620 FOR I=1 TO N0 :REM Search VC for any points on
1630 IF L-VC(I)<>1 GOTO 1650 :REM current line.
1640 M$=MID$(STR$(999+M*L1+TC(I)),3) :REM Calculate tab, M$.
1650 P$=P$+"0;" + M$ + "xxx" :REM Print a square for theory points.

```

```
1660 NEXT I
1670 P#=P#+"1" :REM Advance one vertical dot.
1680 NEXT K
1690 LPRINT P#;
1700 LPRINT CHR$(29); :REM Exit graphics.
1710 NEXT J
1720 NEXT N :REM Current line is now complete.
1730 REM
1740 REM ;;;;;;;;;;;;;;;;;;;;;;;;;;;;;;;;;;;;;;;;;;;;;;;;;;;;;;;;;;;;;;;;;;;;;;;;;
1750 REM ; This section prints the lower margin with title.
1760 REM ;;;;;;;;;;;;;;;;;;;;;;;;;;;;;;;;;;;;;;;;;;;;;;;;;;;;;;;;;;;;;;;;;;;;;;;;;
1770 REM
1780 LPRINT CHR$(28);"0;" +ML#+CHR$(127);
1790 FOR I=2 TO N3*L1 :REM Print lower margin
1800 T=I*A/N3/L1+T1 :REM using vertical bars to give scale,
1810 IF T-D1*INT(T/D1)<A/N3/L1 THEN LPRINT CHR$(127); ELSE LPRINT "A";
1820 NEXT I
1830 LPRINT CHR$(127);CHR$(29)
1840 FOR I=0 TO N3
1850 T=I*A/N3+T1+.001 :REM and labels in even 5's and 10's.
1860 IF T-D1*INT(T/D1)<A/N3 THEN LPRINT TAB(I+M-1);INT(T/D1)*D1;
1870 NEXT
1880 LPRINT:LPRINT
1890 LPRINT TAB(35);"TEMPERATURE (K)"
1900 LPRINT:LPRINT
1910 LPRINT "CONSTANT=";C;" BARRIER=";B1
1920 REM
1930 REM Repeat fit attempt request follows.
1940 REM
1950 INPUT "Recalculate";Y#
1960 IF STRING$(1,Y#)="Y" GOTO 450
1970 END
```